AlN Thin Film Electroacoustic Devices

BY

GONZALO FUENTES IRIARTE

A
Sabina Iriarte Ilintxeta,
mi madre.

Dissertation for the Degree of Doctor of Philosophy in Solid State Electronics presented at Uppsala University in 2003

ABSTRACT

Iriarte, G.F. 2003. AlN Thin Film Electroacoustic Devices.
Acta Universitatis Upsaliensis. *Comprehensive Summaries of Uppsala Dissertations from the Faculty of Science and Technology.* 817. 67pp. Uppsala. ISBN 91-554-5557-3

Recently, the enormous growth in personal communications systems (PCS), satellite communication and various other forms of wireless data communication has made analogue frequency control a key issue as the operation frequency increases to the low/medium GHz range. Surface acoustic wave (SAW) and bulk acoustic wave (BAW) electroacoustic devices are widely used today in a variety of applications both in consumer electronics as well as in specialized scientific and military equipment where frequency control is required. Conventional piezoelectric materials such as quartz, $LiNbO_3$ and $LiTaO_3$ suffer from a variety of limitations and in particular medium to low SAW/BAW velocity as well as being incompatible with the IC technology. Thin piezoelectric films offer the great flexibility of choosing at will the substrate/film combination, thus making use of the electroacoustic properties of non-piezoelectric substrates, which widens greatly the choice of fabrication materials and opens the way for integration of the traditionally incompatible electroacoustic and IC technologies.

This thesis focuses on the synthesis and characterization of novel thin film materials for electroacoustic applications. A prime choice of material is thin piezoelectric AlN films which have been grown using both RF and pulsed-DC reactive sputter deposition on a variety of substrate materials. A unique synthesis process has been developed allowing the deposition of high quality AlN films at room temperature, which increases greatly the process versatility. The films are fully c-axis oriented with a 1.6° FWHM value of the rocking curve of the AlN-(002) peak. Complete process flows for the fabrication of both SAW and BAW devices have been developed. Electroacoustic characterization of 2 GHz BAW resonators yielded an electromechanical coupling coefficient (k_t^2) of 6.5%, Q-value of 600 and a longitudinal velocity of 11350 m/s. AlN thin films based SAW resonators on SiO_2/Si yielded a SAW velocity of around 5000 m/s and a piezoelectric coupling coefficient (K^2) of around 0.3%. Finally, AlN on polycrystalline diamond 1 GHz SAW resonators exhibited an extremely high SAW velocity of 11800 m/s, a piezoelectric coupling coefficient (K^2) of 1% and a Q-value of 500.

G.F.Iriarte, Solid State Electronics, The Ångström Laboratory
Uppsala University, Box 534, SE-751 21 Uppsala, Sweden

Publications

This thesis is based on the following publications, which in the following will be referred to in the text by their Roman numerals.

I. Synthesis of highly oriented piezoelectric AlN films by reactive sputter deposition
F. Engelmark, G. Fuentes, I. V. Katardjiev, A. Harsta, U. Smith, and S. Berg
J. Vac. Sci. Technol. A, Vol. 18, No. 4, Jul'Aug 2000

II. Structural and electroacoustic studies of AlN thin films during low temperature radio frequency sputter deposition
F. Engelmark, G. F. Iriarte, I. V. Katardjiev, M. Ottosson, P. Muralt, and S. Berg
J. Vac. Sci. Technol. A 19(5), Sep'Oct 2001

III. Selective etching of Al/AlN structures for metallization of surface acoustic wave devices
F. Engelmark, G. F. Iriarte, and I. V. Katardjiev
J. Vac. Sci. Technol. B 20(3), May'Jun 2002

IV. Reactive sputter deposition of highly oriented AlN films at room temperature
G. F. Iriarte, F. Engelmark, I.V. Katardjiev
J. Mater. Res. 17(6), (2002) 1469-75

V. Influence of deposition parameters on the stress of magnetron sputter-deposited AlN thin films on Si (100) substrates.
G. F. Iriarte, F. Engelmark, M. Ottosson , I.V. Katardjiev.
J. Mater. Res. 18(2), (2003)

VI. Electrical Characterization of AlN MIS- and MIM-structures
F. Engelmark, J. Westlinder, G. F. Iriarte, I. V. Katardjiev, J. Olsson
Submitted to IEEE- Transactions on Electron Devices (2002)

VII. Synthesis of C-Axis Oriented AlN Thin Films on Metal Layers: Al, Mo, Ti, TiN and Ni.
G. F. Iriarte, J. Bjurström, J. Westlinder, F. Engelmark, I.V. Katardjiev.
Submitted to IEEE- Transactions on Ultrasonics, Ferroelectrics and Frequency Control (2002)

VIII. SAW propagation characteristics of AlN thin films grown on polycrystalline diamond substrates at room temperature.
G.F.Iriarte
Submitted to Journal of Applied Physics 3 February 2003. Accepted 3 March 2003.

IX. SAW COM-parameter extraction in AlN/diamond layered structures.
G. F. Iriarte, F. Engelmark, I.V. Katardjiev, V.Plessky, V.Yantchev
Submitted to IEEE- Transactions on Ultrasonics, Ferroelectrics and Frequency Control (2003)

Contents

1. Introduction

Acoustic wave devices based on piezoelectric materials have been in commercial use for over 60 years[1]. They are used in a wide variety of applications such as delay lines, oscillators, resonators, sensors, actuators, acoustic microscopy as well as in specialized military equipment but by far the largest market is the telecommunication industry, primarily for wireless communication in mobile cell phones and base stations. This industry consumes annually approximately three billion acoustic wave filters for frequency control. The filters are typically based on surface acoustic wave (SAW) and bulk acoustic wave (BAW) resonator technology. Commonly used piezoelectric materials in SAW devices are single crystalline substrates of quartz (SiO_2), lithium tantalate ($LiTaO_3$) and lithium niobate ($LiNbO_3$). Other well-established resonator technologies are standard on-chip LC, transmission lines and ceramic resonators.

Recently, the enormous growth in personal communications systems (PCS), satellite communication and various other forms of wireless data communication has made analogue frequency control a key issue as the operation frequency increases to the low/medium GHz range. Also, the technological drive to minimise and improve the capacity of such systems has shown the need for the development of high performance, miniature, on-chip filters operating in the low and medium GHz frequency range. At the frequency of interests, other resonator technologies such as LC, ceramic resonators and transmission line resonators become too large for wireless applications[2].

One of the biggest disadvantages of the electroacoustic technology in the microwave region is that it makes use of bulk single crystalline piezoelectric materials, the choice of which is rather limited and which by definition are incompatible with the IC technology. In addition, the properties of these materials determine uniquely the acoustic velocity, which in turn together with the device dimensions define the operating frequency. Thus, the only way to increase the latter is to decrease the device dimensions which comes at an enormous increase in the fabrication costs, both for BAW and SAW devices particularly in the microwave region. In recent years thin piezoelectric films have been developed to extend electromechanical SAW and BAW devices to much higher frequencies[3, 4]. The standard electroacoustic technology, however, continues and will continue to dominate the market for devices operating, say, under 2 GHz. For higher frequencies up to 20 GHz, on the other hand Thin Film Bulk Acoustic Resonators (TFBAR or FBAR) is considered to be the most promising approach today because they are characterised by small dimensions, low losses, high power handling capabilities and not the least low fabrication cost. In addition, this approach allows the great flexibility of choosing at will the substrate/film combination, thus making use of the electroacoustic properties of the non-piezoelectric substrate and widening greatly the choice of fabrication materials. Thus, a whole new variety of thin piezoelectric films can be grown on arbitrary substrates. This approach also makes use of the highly developed thin film technology, where thin films of extremely high uniformity and controlled properties can be grown on large area

substrates. Agilent Technologies[5] is the first company to start mass production of discrete FBAR devices in Q1 2001.

It should be strongly pointed out, however, that by far the greatest potential of using thin films for the fabrication of FBARs is that it opens the very promising possibility of integrating the traditionally incompatible IC and electroacoustic technologies. This in turn will bring about a number of substantial benefits such as significant decrease in the fabrication cost of the final device, easier and simpler device design as well as increased sensitivity, reduced losses, power consumption, device size, materials use, electromagnetic contamination, etc. Another very significant benefit of this integration would be the mass fabrication of highly sensitive, low cost integrated chemical and biological sensors and electronic tags. Environmental control is becoming of great importance for today's society both for the manufacturing industry and public activities. The increasing threat of chemical and biological sabotage along with that of hazardous industrial incidents necessitate large scale monitoring of the environment which can only be done by mass produced low cost sensors.

Thus, the research in this field is centred around the development of novel functional materials (piezoelectric, ferroelectric, etc) with superior electroacoustic properties allowing the fabrication of high frequency devices with improved performance and at the same time at low fabrication cost. By the way of example, materials with high piezoelectric coefficients are sought to allow the design of bandpass filters with large bandwidths, say of the order of 10% or more. Further, these materials should exhibit low electroacoustic losses, i.e. should be characterised with a high quality factor as well as high thermal stability in the temperature range of operation. Tunability is also a desirable property for advanced frequency agile and adaptive microwave communications systems. Not the least, the synthesis process should be compliant with the planar technology, while the materials themselves should be compatible with the IC technology.

This thesis focuses on the synthesis of highly textured piezoelectric thin AlN films using reactive sputter deposition as well as their electrical and electroacoustic characterisation in view of electroacoustic applications. Among the major goals of the work are the development of a low temperature synthesis process of c-axis oriented AlN films, development of a fabrication process flow of thin film based resonators (both SAW and BAW), as well as design, fabrication and characterisation of the latter.

The thesis is organised as follows. Chapter 2 presents a summary of the main theoretical models used for the design, description, parameter extraction and characterisation of the thin film resonators. Chapter 3 gives an overview of the fabrication processes used for the fabrication of thin film electroacoustic devices. Finally, Chapter 4 presents a summary of the major results obtained and published in each paper in this thesis in the order of publication.

PROPERTIES OF ALUMINIUM NITRIDE (ALN)

Aluminium nitride (AlN) thin films are widespread applied because they had some excellent properties such as chemical stability, high thermal conductivity, electrical isolation, a wide band gap (6.2 eV), a thermal expansion coefficient similar to that of GaAs, and a higher acoustic velocity. Therefore, AlN thin films were applied not only to surface passivation of semiconductors and insulators, but also to optical devices in the ultraviolet spectral region, acousto-optic (AO) devices, and surface acoustic wave (SAW) devices.

Polycrystalline films exhibit piezoelectric properties and can be used for the transduction of both bulk and surface acoustic waves. If compared to other piezoelectric film, such as the well known ZnO, AlN shows a slightly lower piezoelectric coupling; its Rayleigh wave velocity is close to the maximum in the range of values of most materials, being that of ZnO close to the minimum. The Rayleigh wave phase velocity in c-cut AlN (V_{ph} = 5607m/s) is much higher than that of most substrates of practical interest in SAW devices technology.

This suggests that AlN and ZnO, rather than alternatives, have to be considered each with its own field of application, with a preference for AlN in high Rayleigh wave velocity substrates and high frequency applications.

As to sputter film growth, conditions are more critical for AlN then for ZnO because of the possible presence of strong internal stresses (see Paper V). Results have shown that the growing of high thickness AlN films is rather critical because of its tendency to present microcracking. This tendency is more evident with increasing the thickness of the film and when using silicon substrates, particularly in the (100) orientation.

Property	Value
Band gap	6.2 eV
Density	3.3 g/cm3
Theoretical thermal conductivity	320 W/m-K
Thermal expansion coefficient	4.6E-6/ ºC
Critical field strength Ec	6-15 MV/cm
Relative dielectric constant εr	8.5
Refractive index n	2.15
Thermal conductivity	2.0 W/cmK
Melting point	>2000 ºC
Lattice constant a	3.112 Å
Lattice constant c	4.982 Å

Table 1   Some data on AlN

AlN has a very large volume resistivity. It is a hard material with a bulk hardness similar to quartz, about 2.000 Kg/mm. Pure AlN is chemically stable to attack by atmospheric gases at temperatures less than about 700 ºC. The combination of these physical and chemical properties has stirred considerable interest in practical application of AlN both in bulk and thin-film form.

2. Theoretical aspects

2.1. Acoustic Wave Excitation

In a piezoelectric medium, the stress (T) and the electric displacement (D) depend linearly on both the strain (S) and the electric field (E), and the equations for D and T become:

(1)
$$T_{ij} = c_{ijkl}^{E} \cdot S_{kl} - e_{kij} \cdot E_{k}$$

(2)
$$D_{i} = e_{ijk} \cdot S_{jk} + \varepsilon_{ij}^{S} \cdot E_{j}$$

where ε_{ij}, e_{ijk} and C_{ijkl} are the permittivity, piezoelectric and stiffness tensors respectively. These are called the **constitutive equations** or equations of state of the system. The superscript E in the stiffness constants denotes that it is measured at constant electric field.

Due to the piezoelectric effect, the velocity of propagation of acoustic waves in piezoelectric media is higher than in the non-piezoelectric case. It is a common practice to modify the stiffness tensor by adding to it elements of the piezoelectric and permittivity tensors as shown in (3), in order to calculate the impact of piezoelectricity in the velocity of propagation of the wave. The stiffness constants in that case are referred to as "stiffened". However, a specific crystal may be strongly piezoelectric for a given propagation direction while the effect is completely absent in another direction. Hence, piezoelectricity is always "coupled" to the direction of propagation or "cut" of the crystal. For this reason, Euler angles[6] are often used in the literature to render the stiffened stiffness constants into a specific propagation direction[7]. Hence, piezoelectric corrections to the stiffness matrix depend not only on the permittivity [ε] and piezoelectric [e] matrices, which in turn depend on the symmetry class of the material, but also on the direction of propagation of the acoustic wave. For a piezoelectrically stiffened acoustic wave, the phase velocity is determined by

(3)
$$V_{ph}' = \frac{\omega}{k} = \sqrt{\frac{C^{E}}{\rho}\left(1 + \frac{e^{2}}{\varepsilon^{S}C^{E}}\right)}$$

where the subscripts of the tensor components have been dropped for clarity.

To determine the piezoelectric correction quantitatively, we use the unstiffened phase velocity

(4)
$$V_{ph} = \frac{\omega}{k} = \sqrt{\frac{C^{E}}{\rho}}$$

Rewriting the stiffened phase velocity (3) in terms of the unstiffened phase velocity we obtain

(5)
$$V_{ph}' = V_{ph}\left(1 + K^{2}\right)^{\frac{1}{2}}$$

where the constant K^{2} is given by

(6) $$K^2 = \frac{e^2}{\varepsilon^S C^E}$$

and is called the piezoelectric coupling constant.

We also define the electromechanical coupling constant:

(7) $$k_t^2 = C^D = C^E + \frac{e^2}{\varepsilon^S}$$

where the subscript refers to the requirement that the electric field is applied across the thickness of the crystal. Clearly, the coupling constants k_t *and* K^2 are related as

(8) $$k_t^2 = \frac{K^2}{1+K^2}$$

The reason for the definition of two different types of coupling constants is explained as follows:

Basically, plane acoustic waves can be excited in piezoelectric crystals using two different configurations referred to as Lateral Field Excitation (LTE) and Thickness Excitation (TE). The stiffening correction term (in brackets in (3)) involves vectors that correspond to the orientation of the acoustically generated electric field. In TE, these vectors are oriented in the direction of acoustic propagation. In LFE, the vectors are in the direction of the external electric field, which can be oriented arbitrarily in the plane perpendicular to the acoustic propagation.

a) Thickness Excitation

In Thickness Excitation, an externally generated electric field in the Z-direction in Figure 1 causes the propagation of an acoustic wave in that direction. The implication of the quasistatic approximation (see below) is that the electric field continuously being generated by the strain wave (i.e. acoustically generated) is longitudinal and propagates at the acoustic phase velocity. The internally generated electric field vector is parallel to both the externally applied electric field and the direction of acoustic wave propagation.
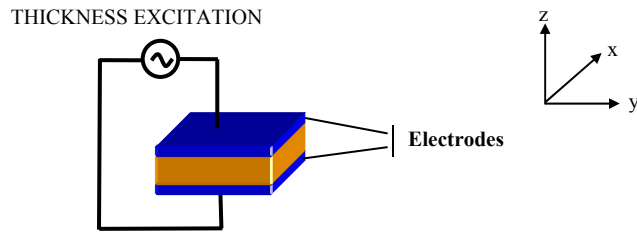
Figure 1   *Thickness Excitation (TE) mode.*

Since the curl of the electric field is zero in the quasistatic case, it implicitly means that the electric displacement vector in the direction of acoustic wave propagation is also zero. This can be shown by considering the characteristic

behaviour of a plane acoustic wave travelling in the Z-direction (i.e. the displacement vector and the stress vary only in the Z-direction), thus having a exp [j(ωt - βz)] dependence. Combining of the constitutive equations (1) and (2) and solving for the displacement we get

$$(9) \qquad D_i = e_{ijk} \cdot S_{jk} + \varepsilon_{ij}^S \cdot \left(-\frac{T_{ij}}{e_{kij}} + \frac{c_{ijkl}^E}{e_{kij}} S_{jk} \right)$$

Since the only displacement components are in the Z-direction, the strain reduces to

$$(10) \qquad S_{jk} = S_z = \frac{\partial u_z}{\partial z} = -jku_z$$

and Newton's law becomes

$$(11) \qquad \rho \frac{\partial^2 u_z}{\partial t^2} = \frac{\partial T_z}{\partial z} = \frac{\rho \omega^2}{-jk}$$

Hence,

$$(12) \qquad D_i = e \cdot (-jku_z) + \varepsilon^S \cdot \left(-\frac{\rho \omega^2}{-jke} + \frac{C^E}{e}(-jku_z) \right)$$

where the subscripts of the tensor components have again been dropped for clarity.

Substituting the expression for the piezoelectrically stiffened phase velocity (3) into this equation we find that $D_z = 0$. The consequence of a vanishing D_z is that in the piezoelectric medium there is a longitudinal electric field without a proportional electric displacement vector. The electrical source does not directly cause a displacement vector (and thus there is no displacement current) in the direction of propagation of the acoustic wave. In other words, it is impossible to extract electric energy from the piezoelectric medium, because there is no displacement current. Energy conversion is accomplished by using resonating structures.

Since the electric field is variable, the stiffness components are measured at constant (zero) electrical displacement D, which explains the use of C^D in place of

C^E.

In the TE mode, the propagating acoustic wave generates an electric field in the piezoelectric crystal and viceversa. Hence the wave propagation is regarded as stiffened and the coefficient, given by k_t, is used to express the coupling in BAW devices using this excitation mode.

b) Lateral Field Excitation (LTE)
In LFE the electric field is in the plane perpendicular to acoustic propagation. A practical realization of Lateral Field Excitation is shown in Figure 2. The applied (external) electric field is uniform in the Y-direction and the propagation of bulk acoustic waves is in the Z-direction (perpendicular to the electric field). An electric field can excite an acoustic wave normal to its direction because the piezoelectric matrix [e] couples electrical and mechanical fields of different orientations.

In Lateral Field Excitation, the internally generated electric field may be accurately assumed to be zero. Hence, the potential Φ is also assumed to be zero. Instead, there is an internally generated electrical displacement vector containing terms that are normal to the direction of acoustic propagation direction and thus parallel to the externally generated electric field. The interaction of the acoustic wave with the source occurs though the electric displacement D, which means that D propagates at the acoustic velocity. The internally generated D vector is parallel to the externally generated electric field vector E. For this reason, in the Lateral Field Excitation mode, the components of stiffness tensor are measured at constant electric field E, which is denoted as C^E.
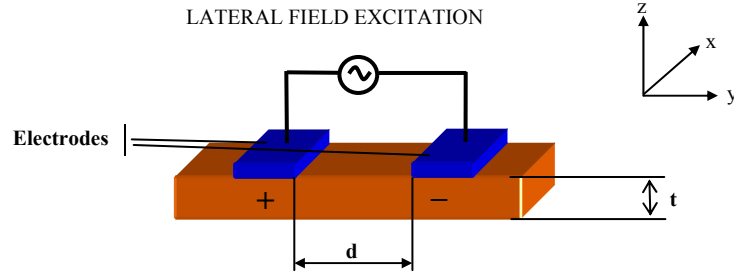

Figure 2 *Lateral Field Excitation (LFE) mode.*

A necessary condition for LFE to exist is that the thickness **t** of the crystal in Figure 2 must be much smaller that the distance between the electrodes **d**. Lateral Field Excitation is relevant to static measurements or to dynamic behaviour of piezoelectric crystals that are very small compared to the acoustic wavelength (i.e. t is much smaller than the distance between the electrodes d), but it is not applicable to wave propagation problems where the variables of interest are time-dependent as they vary with the acoustic wave.

However, due to the analogy in terms of practical realization of devices working in the LFE mode, the coupling constant K^2 (see Equation (5) above) is used to express the coupling in SAW devices. There is a simple interpretation for K^2 in terms of the ratio of externally generated electric field energy density to the mechanical energy density[4].

2.2. Layered structures for SAW applications

2.2.1. Theoretical background

In a piezoelectric material, surface acoustic waves can be generated and detected electrically by means of metal electrodes at the surface. This principle is used in interdigital transducers (IDTs) and multistrip couplers. If an alternating electric field is applied between the electrodes of an IDT, and as a consequence of the piezoelectric effect, surface acoustic waves will travel away from the transducer in both directions. At the frequency for which the acoustic wavelength is equal to the period of the IDT, the electric field between adjacent electrodes will reach the highest level and all the electrodes will contribute to the generation of the acoustic wave in a cooperative manner. Hence, at that particular frequency, often referred to as the center or the Bragg frequency, electromagnetic waves applied are converted into an acoustic signal with maximal efficiency.
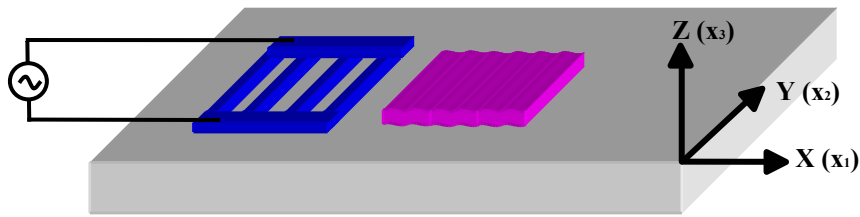
Figure 3 *IDT launching an acoustic wave on a piezoelectric substrate. The coordinate system used is shown to the right.*

In order to derive the equations governing the propagation of acoustic waves in piezoelectric media (equations of motion), we recall the following assumptions:

a) The quasistatic approximation
When either of the media through which an acoustic wave propagates is piezoelectric, the problem involves not only the elastic particle displacements but also the electric and magnetic fields, with the result that the applicable equations are combinations of the elastic equations of motion and of Maxwell's equation, intercoupled by the piezoelectric tensors of the media. The intercoupling is usually weak enough for the solutions of the equations to be divided into two classes, those that propagate with acoustic velocities (a few thousand meters per second) and those that propagate with electromagnetic velocities (~100.000 kilometres per second). We will restrict the discussion here to the former class. With this restriction, the magnetic fields can be neglected and the electric fields can be derived from a scalar potential. In other words, since acoustic waves in commonly used materials are about five orders of magnitude slower than electromagnetic

waves, the piezoelectrically coupled electric field is assumed to be quasistatic. This assumption is known as the quasistatic approximation. Hence,

$$(13) \qquad E_i = -\frac{\partial \Phi}{\partial x_i}$$

For charge-free dielectrics eq.(13) yields:

$$(14) \qquad \frac{\partial D_i}{\partial x_i} = 0$$

Here, E_i is electric field, D_i is electrical displacement, Φ is potential.

b) The mechanical equation of motion

Newton's second law gives the mechanical equations of motion and for an infinitesimally small volume (i.e. the solid is considered as a continuum medium) it states:

$$(15) \qquad \rho \frac{\partial^2 u_i}{\partial t^2} = \sum_{j=1}^{3} \frac{\partial T_{ij}}{\partial x_i}$$

Here, T_{ij} is the stress, and u_i denotes particle displacement. In these equations, the summation convention for repeated indices is employed and the tensors are expressed by Einstein's convention.

Taking the former assumptions into account, the first derivative of the constitutive relation (equations (1) and (2)) with respect to space, leads us to a set of four coupled wave equations; one for the electric potential Φ and three for the three components of the elastic displacement u_i. These are called the wave equations or equations of motion of the system.

$$(16) \qquad \rho \frac{\partial^2 u_j}{\partial t^2} - c_{ijkl} \frac{\partial^2 u_k}{\partial x_i \partial x_l} - e_{kij} \frac{\partial^2 \Phi}{\partial x_i \partial x_k} = 0$$

$$(17) \qquad e_{ikl} \frac{\partial^2 u_k}{\partial x_i \partial x_l} - \varepsilon_{ik} \frac{\partial^2 \Phi}{\partial x_i \partial x_k} = 0$$

Thus, the equations of motion are derived from the constitutive equations of the media after substituting Newton's second law and the quasistatic approximation.

Following Campbell and Jones method[8], the general solution to the wave equation above is assumed to be a linear combination of partial waves given by

$$(18) \qquad u_j = \alpha_j \cdot e^{ikbx_3} \cdot e^{ik(x_1 - vt)} \qquad\qquad , j = 1,2,3$$

$$(19) \qquad \Phi = \alpha_4 \cdot e^{ikbx_3} \cdot e^{ik(x_1 - vt)}$$

where the constants α give the relative amplitudes of the displacement components of each partial wave and the decay constants b describe the variation with depth of the amplitude and phase of the partial wave measured on a "plane of constant phase" i.e. a plane perpendicular to the XZ-plane in Figure 3. Substituting the partial waves into the wave equation an eighth-order algebraic equation in the decay constants b is obtained. Thus, for each value of the phase velocity V_{ph}, eight

values of b are found in the most general case. Moreover, for each of the eight roots b, there is a four-component eigenvector (α_1, α_2, α_3, α_4). When the system is irreductible, it is not always possible to find a solution with the full number of arbitrary functions, but it is possible to construct solutions that contain as many constants as required. In other words, since we have 8 different decay constants b and for each one of this constants b, there is a unique eigenvector (α_1, α_2, α_3, α_4), we must find a way to determine one solution (now there are 8 possible solutions). The way to find this unique solution is by combining all the partial waves using weighting factors C_m. This weighting factors can be find out by determining as many boundary conditions as necessary, that means, as many boundary conditions as weighting factors C_m appear in the equation system.

The particle displacement and potential in the equations for the partial waves, Equations (18) and (19), are given as eight linear combinations of plane waves. These linear combinations constitute the general solution of the system:

$$(20) \qquad u_j = \sum_{m=1}^{8} C_m \alpha_j^m \cdot e^{ikb^m x_3} \cdot e^{ik(x_1 - vt)} \qquad\qquad , j=1,2,3.$$

$$(21) \qquad \Phi = \sum_{m=1}^{8} C_m \alpha_4^m \cdot e^{ikb^m x_3} \cdot e^{ik(x_1 - vt)}$$

So far, the discussion concerns bulk materials. For layered structures, another set of boundary conditions must be satisfied at the interface between adjacent layers. Since the assumption of the semi-infinite substrate is only applicable for the lowest layer, eight unknown constants exist for each layer except for the lowest one. This is so because at the interface between two layers of different materials, the wave is likely to be reflected back towards the surface, hence giving rise to positive values of the decay constants b. For instance, in the case of AlN/diamond structure (studied in Paper VIII and Paper IX), the general solution for the displacement and the potential satisfying (16) and (17) are given as

$$(22) \qquad u_j^{Dia} = \alpha_j^{Dia} \cdot e^{ikb_{Dia} x_3} \cdot e^{ik(x_1 - vt)}$$

$$(23) \qquad \Phi^{Dia} = \alpha_4^{Dia} \cdot e^{ikb_{Dia} x_3} \cdot e^{ik(x_1 - vt)}$$

$$(24) \qquad u_j^{AlN} = \alpha_j^{AlN} \cdot e^{ikb_{AlN} x_3} \cdot e^{ik(x_1 - vt)}$$

$$(25) \qquad \Phi^{AlN} = \alpha_4^{AlN} \cdot e^{ikb_{AlN} x_3} \cdot e^{ik(x_1 - vt)}$$

where α_j^{Dia} (j = 1,2,3) and α_j^{AlN} (j = 1,2,3) are constants. Substituting (22) and (23)into (16) and (17) respectively, the eighth-order equation is obtained for b_{Dia} and the eight roots are obtained. Similarly, substituting (24)and (25) for an AlN layer into (16) and (17) respectively, the eighth-order equation is obtained for b_{AlN} and eight roots are obtained. Therefore, the displacement u_j and the potential Φ are expressed as the summation of the linear combinations of eight waves, which are given as

$$(26) \qquad u_j^{Dia} = \sum_{m=1}^{8} C_m^{Dia} \alpha_j^{Dia(m)} \cdot e^{ikb_{Dia}^{(m)}x_3} \cdot e^{ik(x_1-vt)} \qquad , j=1,2,3.$$

$$(27) \qquad \Phi^{Dia} = \sum_{m=1}^{8} C_m^{Dia} \alpha_4^{Dia(m)} \cdot e^{ikb_{Dia}^{(m)}x_3} \cdot e^{ik(x_1-vt)}$$

$$(28) \qquad u_j^{AlN} = \sum_{m=1}^{8} C_m^{AlN} \alpha_j^{AlN(m)} \cdot e^{ikb_{AlN}^{(m)}x_3} \cdot e^{ik(x_1-vt)} \qquad , j=1,2,3.$$

$$(29) \qquad \Phi^{AlN} = \sum_{m=1}^{8} C_m^{AlN} \alpha_4^{AlN(m)} \cdot e^{ikb_{AlN}^{(m)}x_3} \cdot e^{ik(x_1-vt)}$$

Because 90% of the SAW energy concentrates within one wavelength near the surface of the substrate, thick (at least 3 times the acoustic wavelength) piezoelectric substrates are assumed to be semi-infinite substrates. Assuming that the diamond layer is a bulk material (i.e. semi-infinite), four out of the eight b roots are effective to satisfy the condition that the SAW wave does not exist at negative infinity for $-X_3$ (see Figure 3). Therefore, (26) and (27) are expressed as follows.

$$(30) \qquad u_j^{Dia} = \sum_{m=1}^{4} C_m^{Dia} \alpha_j^{Dia(m)} \cdot e^{ikb_{Dia}^{(m)}x_3} \cdot e^{ik(x_1-vt)} \qquad , j=1,2,3.$$

$$(31) \qquad \Phi^{Dia} = \sum_{m=1}^{4} C_m^{Dia} \alpha_4^{Dia(m)} \cdot e^{ikb_{Dia}^{(m)}x_3} \cdot e^{ik(x_1-vt)}$$

For the AlN layer, all eight roots apply. From Equations (28) to (31) it is seen that a total of twelve unknown parameters (four corresponding to the diamond layer and eight corresponding to the AlN layer) appear for the AlN/Diamond structure.

Once the equations describing the system have been erected, **boundary conditions** have to be applied to solve it. These are as follows:

The particle displacements and the traction components of stress (T_{13}, T_{23} and T_{33}) must be continuous across the interface because of the intimate nature of the contact assumed between the two materials. Since the surface is assumed to be mechanically stress free, the three traction components of stress must vanish thereon. The electrical boundary conditions to the problem are provided by the continuity of the potential and of the normal component of electric displacement across both the interface and the free surface.

In the case of a layered structure, the conditions of each layer boundary are also required for u, T, D, and the potential for being continuous. For instance, the following conditions apply for the AlN/diamond system at the boundary interface.

$$(32) \qquad u_i^{Dia} = u_i^{AlN}, T_{i3}^{Dia} = T_{i3}^{AlN}, D_i^{Dia} = D_i^{AlN}, \Phi^{Dia} = \Phi^{AlN}$$

We are left with twelve boundary conditions for the general problem under consideration. It is convenient to group these boundary conditions into three categories:

- the mechanical boundary conditions involving transverse displacements and facial stresses,
- the remaining electrical boundary conditions, and

▪   the sagittal plane (XZ-plane in Figure 3) mechanical boundary conditions.

For the twelve unknown parameters, three equations are given by the stress boundary condition at the surface of AlN and one equation is given by the potential at the surface or the electrical displacement boundary condition. Three equations are obtained by the stress boundary condition and three equations by the continuity of each displacement at the interface between diamond and A1N. From the continuity of the normal direction of the electric displacement and the conductivity of the potential at the interface between diamond and A1N, two additional equations are obtained. Hence, the equation system can be solved since it consists of twelve equations with twelve unknown parameters.

Substituting this general solution into the wave equation and taking into account the boundary conditions yields the boundary-condition determinant for the general case. Making this determinant equal zero by choosing values of the phase velocity V_{ph} until it is so, we can find out all coefficients b and all coefficients α. After that, the twelve weighting factors C_m can easily be found since we have twelve equations for twelve unknowns C_m and the general expressions for the displacement and for the potential are completely defined.

A detailed description of the propagation of acoustic waves in layered structures can be found in Farnell and Adler's work[9-12], which in its turn has its origin on Campbell and Jones method[8]. Adler's group at McGill Univ., Montreal, Canada, has developed a computer program[13-15] based on this approach, which is available on the internet at UFFC website (www.ieee-uffc.com).

2.2.2. Dispersion curves

The method described is very useful in the design process of SAW devices since it permits to calculate the propagation velocity of the acoustic wave in a given direction in the material. Moreover, since the values of the phase velocity depend on the decay constants b, it is clear that the velocity of the acoustic wave will depend on the thickness of the layer of material though which it propagates, in other words, it will be dispersive. The determination of the exact velocity of propagation of the acoustic wave is essential in the design process since it determines the center frequency of the device. Acoustic losses can be accounted for in the model by including the viscous damping of the medium which in practice is implemented by introducing complex stiffness constants[7]. Another very important result is the possibility to calculate the piezoelectric coupling coefficient, a parameter of primary importance for the design of electroacoustic devices.

In a layered surface acoustic wave device, where an array of electrode stripes is used to excite the acoustic wave, the location of the electrodes with respect to the layers can drastically affect the coupling coefficient of the device. Basically, four different electrode/layer combinations are possible as shown in Figure 4.
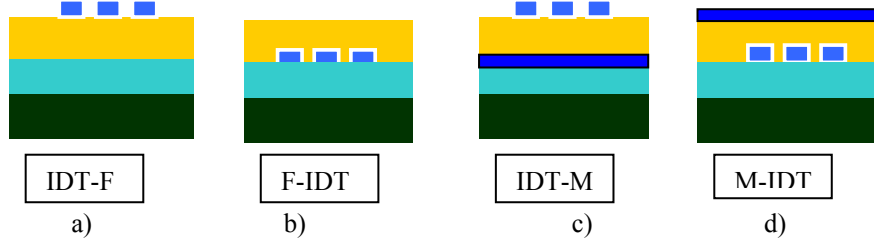
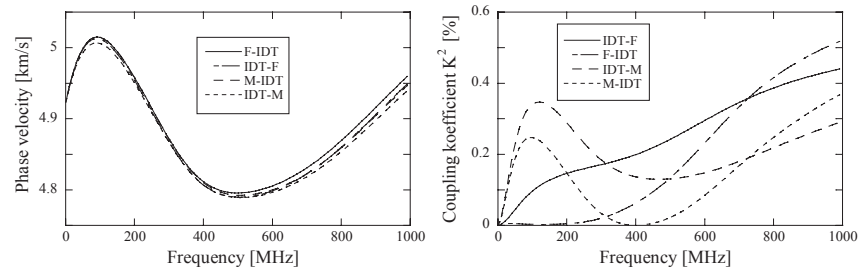**Figure 4** *Different IDT/Thin Film configurations.*

They are explained as follows:

- Case 1: IDT-F means that the IDT's are located on top of the piezoelectric film without a short circuiting plane
- Case 2: F-IDT means that the IDT's are located under the piezoelectric film without a short circuiting plane
- Case 3: IDT-M means that the IDT's are located on top of the piezoelectric film with a short circuiting plane under the latter
- Case 4: M-IDT means that the IDT's are located under the piezoelectric film with a short circuiting plane on top of the latter

As discussed above (see Section 2.1, Eq. (3)), the following relations are well known for piezoelectric materials.

$$(33) \qquad K^2 = \frac{C_o - C_s}{C_o} = \frac{(V_o)^2 - (V_s)^2}{(V_o)^2} = 2\frac{V_o - V_s}{V_o}$$

where C_o and C_s are stiffness constants and V_o and V_s are the phase velocity of SAW at the electrically open surface (stiffened) and shorted surface (unstiffened), respectively. This approximation is useful to determine the coupling coefficient for SAW. Since V_o and V_s are obtained by the Campbell & Jones method discussed above, K^2 is easily calculated. For example, K^2 of the structure in Figure 4(a) is obtained from the SAW velocity, V_o, calculated by the free surface condition in Figure 4(a), and from the SAW velocity, V_s, calculated for the metallized region shorcircuiting the A1N surface as shown in Figure 4(d).

Figure 5 *Dispersion curves for the coupling coefficient as well as the phase velocity for different IDT configurations.*

By way of example, Figure 5 shows the frequency dependence of the SAW velocity and the coupling coefficient for a thin film structure consisting of 2.1 μm AlN, 0.7 μm SiO_2 deposited on (100) silicon.

2.3. Modelling techniques for SAW Devices.

The complexity of the generation and detection of acoustic waves on a piezoelectric substrate has lead to the development of several different mathematical approaches for its description[16, 17]. In early stages of device development, simple approximate methods may be useful to gain rapid insight on the device performance, without going into details that may not be considered relevant an that point. Two closely related methods referred to as the Delta Function model[18] and the Impulse Response model[19, 20] are classified under this group. On the other hand, a detailed knowledge and description of the electro-acoustic interaction between IDT and substrate is necessary if the specifications on device characteristics are to be fulfilled with high accuracy. In such cases, phenomenological methods can be used to predict details with higher precision, as needed for high performance devices, as well as to gain insight into factors limiting their performance. The Equivalent Circuit model[21-24], the Coupling of Modes (COM) model[25-31] and the P-matrix Model (PMM)[16, 32, 33] are widely used by SAW filter designers for these purposes. Finally, physical methods based on the Green's function approach allow us to gain insight into physical phenomena affecting the device performance such as the use of different acoustic wave modes, anisotropic substrates based on multilayer structures etc. The numerical Green's function methods for the analysis of periodic structures may be classified into two categories. In the eigenmode analysis[34-36], waves propagating freely in electrically open or shorted structures are considered. An unknown phase shift (or wavenumber) in the elastic and electric fields between the successive periods is to be found as a function of frequency. As a result, the dispersion curve is obtained. A limitation of this method is that the coupling to an applied voltage can be analyzed only indirectly. Furthermore, the Green's function for a complex valued wavenumber is required, which demands some additional assumptions on the continuation of the real argument Green's functions into the complex plane[37, 38]. An alternative to the eigenmode analysis is the analysis of the generation problem[32, 39-43]. The system modelled is driven directly by a voltage source and the currents on the electrodes are of interest. Since the generation problem resembles practical experiments and leads to the computation of the electrical admittance of the structure, the results of the generation problem are easier to interpret than those of the eigenmode analysis.

In this thesis, the Coupling-Of-Modes parameters have been extracted for the AlN/Diamond structure as shown in Paper IX. An accurate extraction of the COM parameters is mandatory in order to be able to design SAW devices with superior performance[44]. The parameter extraction may be done either using numerical techniques[45, 46] or directly from experimental measurements of arrays of SAW resonators with varying number of electrodes, apertures and metallisation ratios. COM is a very useful method because of its simple mathematical formalism and its flexibility. It is one of the few models that are capable of describing SAW devices with finite lengths and enables fast computation.

2.4. Modelling techniques for BAW Devices.

The Butterworth Van Dyke (BVD) equivalent circuit is used both for SAW as well as for BAW resonating structures at near resonance. A modification of the circuit by adding a resistance in parallel to the plate capacitance Co as shown in Figure 6 has been reported to improve accuracy[47].
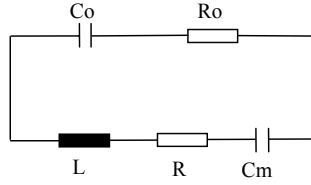
Figure 6 *Modified Butterworth Van Dyke (BVD) equivalent circuit*

The electromechanical coupling coefficient k_t discussed above and the quality factor Q, can be derived from the measured as well as modelled data using the equations

(34) $$k_t = \left(\frac{\pi^2}{4}\right) \cdot \left(\frac{f_p - f_s}{f_p}\right)$$

(35) $$Q_s = \frac{2\pi f_s L}{R}$$

The relative difference in the frequencies f_s and f_p depends on both the material coupling factor and the resonator geometry. For this reason a quantity called the effective coupling factor is used, particularly in filter design literature, as a convenient measure of this difference. The effective coupling constant $k_{t\,eff}$ is given by[48, 49]

(36) $$k_{t\,eff} = \left(\frac{\pi^2}{4}\right) \cdot \left(\frac{f_s}{f_p}\right) \cdot \left(\frac{f_p - f_s}{f_p}\right)$$

The above model is normally used to extract the main electroacoustic parameters of a resonator L, R, C_m, C_o, Q and k_t from measurement data.

Another popular model often used for modelling of FBAR resonators is the Nowotny-Benes model[50] which is a one-dimensional physical description of a resonator consisting of an arbitrarily oriented piezoelectric layer and two electrodes. In this case, the electroacoustic parameters are modelled from knowledge of the materials constant of the materials involved. The model was extended by the authors in 1991 to include an arbitrary number of electrodes[51]. This approach has been used in this thesis to determine parameters such as the coupling and the thickness of the piezoelectric thin film and that of the electrodes for BAW resonators at a given frequency of operation.

3. Process Technology

The process technology for the fabrication of Thin Film Bulk Acoustic Wave Resonators, so-called TFBAR, as well as Thin Film Surface Acoustic Wave Resonators or TFSAR, is presented in this section. All patterning steps performed to manufacture these devices are standard IC-technology processes.

A. PROCESS SCHEME FOR A THIN FILM SAW RESONATOR

A single side polished p-doped silicon wafer is cleaned using a standard RCA procedure. Highly resistive Si is used to reduce electromagnetic feedthrough and parasitic capacitance through the Si wafer. A process scheme for the manufacture of a thin film SAW resonator normally contains the following steps:

- Deposition: e.g. 2µ of highly oriented AlN (aluminum nitride) to form the piezoelectric active layer
- Deposition: 200 nm of aluminum on the top of the AlN to form the IDT electrodes
- Lithography: photoresist spin on top of the metal layer. Exposure. Develop.
- Etch: patterning of the interdigital transducer (IDT)
- Etch: resist removal preferably by ashing
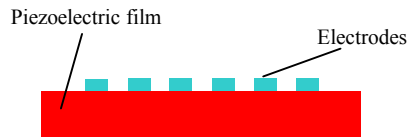
Figure 7 *Schematic illustration of FSAR (side view).*

B. PROCESS SCHEME FOR A THIN FILM BAW RESONATOR

There are basically two types of TFBAR resonators - membrane and solidly mounted resonators (SMR). In the first instance the resonator represents a free standing membrane while in the second case the membrane is solidly mounted onto the substrate but acoustically isolated from the latter by a multilayer stack Bragg reflector.
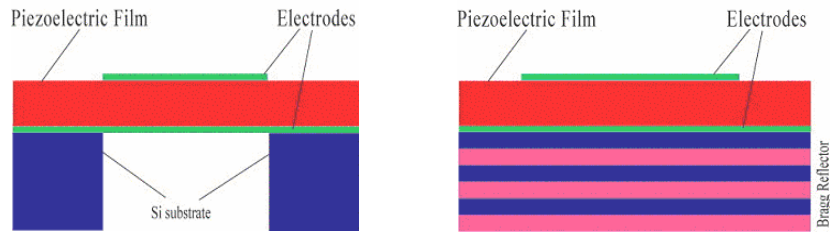
Figure 8   *Schematic illustration of SMR and membrane FBARs*

The SMR approach offers some advantages with respect to the fabrication of the devices but yields a somewhat lower Q-factor. The membrane type, offers a higher quality factor at the expense of higher fabrication cost. In addition, this method opens the possibility for the fabrication of Voltage Controlled Oscillators (VCO). Cavity definition in this case may be done in two ways, namely etch-back (the wafer is etched from the back side) and surface micromachining, where a sacrifical layer under the resonator is etched from the surface. Both methods allow combining materials with opposite thermal coefficients of delay (TCD) thus fabricating devices with high thermal stability.

A typical process etch-back scheme for the fabrication of a membrane type FBAR contains the following steps:

- A double side polished p-doped silicon wafer (the silicon wafer should have a thickness of 300 μm) is cleaned using standard cleaning procedure.
- Deposition: 50 nm of aluminium to form the bottom electrode and to act as an etch stop of the bosch-process
- Deposition: 200 nm of titanium to form the bottom electrode
- Lithography: photoresist spin on top of the metal layer. Exposure. Develop.
- Etch: patterning of the bottom electrode
- Etch: resist removal
- Deposition: 2μ of highly oriented AlN (aluminium nitride): the piezoelectric active layer
- Deposition: 200 nm of titanium to form the top electrode
- Deposition: 50 nm of aluminium to form the top electrode (symmetry of the structure)
- Lithography: photoresist spin on top of the metal layer. Exposure. Develop.
- Etch: patterning of the top electrode
- Etch: resist removal
- Deposition: 200 nm of aluminium on the back side of the wafer to act as mask in the bosh-process

- ▪ Lithography: photoresist spin on top of the metal layer. Exposure. Develop.
- ▪ Etch: patterning of the membrane
- ▪ Etch: from the back of the wafer to finally define the membrane

As seen from the above description the processes listed are standard planar processes. And this is one of the big advantages of the thin film electroacoustic technology, namely its full compatibility with the IC fabrication technology, bringing about substantial functional and economic benefits.

Since a large part of this work deals with developing fabrication processes of both FBAR and FSAR structures the remainder of this section takes a closer look at the processes employed as well as the most widely used analytical methods.

3.1. Low Density Plasmas

Plasma is a partially ionised gas with equal numbers of positive and negative charges. It can also be thought of as a collection of electrons, singly and multiply charged positive and negative ions along with neutral atoms, molecules and molecular fragments. The degree of ionisation is very small; around one charged particle per 10^4 to 10^6 neutral atoms and molecules. To maintain a steady state of electron and ion densities, an ionisation process must balance the recombination process, i.e. an external energy source is required. In practice, that energy source is an electric field, which can act directly on the charged particles only. The positive particles are mainly atoms or molecules that have lost one or more electrons i.e. ions. The majority of the negatively charged particles are free electrons.

The main species generating particles are energetic electrons, which through collisions with neutrals maintain the supply of ions and radical species and generate processes such as

- Ion and electron generation
- Atom and radical generation
- Photon production that gives the plasma its characteristic optical emission

3.1.1. Particle Energies in low density plasmas

At steady state the free electrons acquire a sufficient energy from the applied electric field to produce impact ionisation of the gas at a rate equal to the loss rate. The light electrons, however, cannot transfer efficiently kinetic energy to the much heavier atoms and molecules. This results in that the electrons are not thermalized and hence possess a much higher energy or equivalently "temperature" than the ions.

The fraction of energy transferred in an elastic collision between an electron and an atom or a neutral is of the order of 2 m/M~10^{-4}, where m and M denote the masses of the electron and the atom respectively.

A typical electron temperature is in the range 2-5 eV whereas that of ions and neutrals is a few times the room temperature (0.026 eV). The high electron energy is enough to excite high temperature electron-molecule reactions. Generating the same reactive species without plasma would require temperatures of more than 1000°C. This is the main advantage of plasma processing, the ability to activate high temperature type reactions at low temperature conditions. The plasmas normally used for processing in microelectronics are also called low-temperature plasmas.

The ions easily loose energy via elastic collisions with the rest of the particles in the plasma, which leads to their rapid thermalization. If the ions have high enough energies they will cause significant effects on the grown film, such as resputtering, mixing, enhance surface diffusion as well as generate defects.

3.1.2. Potential distribution in a plasma

Since the electrons have much higher energies they are more mobile than the ions and diffuse more quickly to the surface of any solid in contact with the plasma. Hence, a surface in contact with the plasma will build up a negative potential with respect to the plasma and which potential will repel the low energy electrons such that at equilibrium the ion current is equal to the electron current. In other words, the plasma will always acquire a positive potential with respect to other surfaces, such as the chamber walls. This potential is normally referred to as the **plasma potential V_p.**

Experimentally, a depletion of the plasma edges near the chamberwalls occurs. The plasma edge is visibly more pronounced at a negatively biased electrode where it is usually called the sheath or the dark space. In standard processing conditions the latter can vary between fractions of a millimeter to several millimeters. The positive plasma potential means that any body that is in contact with the plasma will be subjected to ion bombardment with average ion energy equal to that of the plasma potential (unless an additional external electric field is applied). Since the acceleration of the ions occurs in the plasma sheath, which follows the contour of the body, the ion bombardment will generally be normal to the surface. These energetic ions are the driving force for all ion assisted plasma processes.
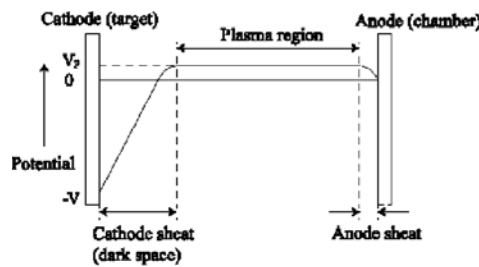
Figure 9 *The potential distribution of a plasma. It is seen that the voltage drop between the plasma and the cathode is by far the greatest in the system.*

3.1.3. DC Plasma discharges

In the cathode sheath, the high mobility of light electrons and the repulsive field cause the electron population in this region to be so depleted that few electronic excitations occur and a glow is therefore not observed (no photons are emitted). For this reason a sheath is also frequently referred to as the "dark space". Sheaths form not only at the cathode surface but also at the anode or at any surface exposed to the plasma as discussed above.

While the surfaces just discussed could be either insulating or conducting, it is important to note that both electrodes in a dc plasma discharge must be conductors since the net current is a dc electron current generated by the second electron emission.

DC plasma discharges suffer from very low deposition rates. In addition, DC plasmas are operated at relatively high pressures and high discharge voltages due to the low ionization efficiency, resulting in even lower deposition rates (due to gas scattering) as well as in higher damage production due to high energetic neutrals.

This can be dramatically improved by using magnetrons as discussed below.

3.1.4. Magnetron sputtering

The use of a magnetic field to enhance the sputtering rate leads to the term magnetron sputtering. Magnetron sputtering is the most widely used method for vacuum thin film deposition. Although the basic diode sputtering method (without magnetron or magnetic enhanced) is still used in some application areas, magnetron sputtering now serves over 90% of the market for sputter deposition. The deposition rate enhanced is commonly a factor of 10 over diode sputtering methods.

The magnetron creates a strong magnetic field close to the target surface. This magnetic field confines the fast electrons to the dark space by forcing them to travel along spiral trajectories due to the Lorentz force

(37) $$F = q(v \times B)$$

Here q is the elementary charge, v is the velocity of the particle, and B is the magnetic field.

Thus, trapping the energetic electrons close to the target surface increases the ionization efficiency of the discharge, which in turn results in higher density plasmas. Due to the much more efficient ionization, the discharge can be sustained at much lower pressures, down to 1 mTorr. Lower discharge pressures mean larger mean free path (λ), resulting in that the particles sputtered from the target retain some of their kinetic energy as they adsorb onto the substrate surface. This excess energy results in increased surface diffusion, and hence film densification and in many cases improved crystal growth as discussed in Paper IV.

3.1.5. RF Plasma discharges.

To allow the sputtering of insulating materials an alternating power is often applied to the electrodes in a diode discharge. In this case the power is coupled capacitively to the plasma and the net DC current through the power supply is zero. There exist two main configurations, symmetric and asymmetric respectively, as defined by the ratio of the electrode areas. The asymmetric case is normally used for sputtering purposes, where the target has a much smaller area than the grounded electrode (chamber walls). It is readily shown that in RF discharges, a negative potential relative the plasma on each electrode is formed and which potential depends in an exponential fashion on the electrode area, i.e.

(38) $$\left(\frac{V_c}{V_d}\right) = \left(\frac{A_d}{A_c}\right)^4$$

where V_c, A_c and V_d, A_d are the respective electrode potentials and areas.

Since the area of the chamber walls is much larger than the target itself, the DC potential on the former is negligibly small, while that on the latter is sufficiently high for sputtering purposes.

High-frequency electric fields cause more efficient ionisation in a discharge than DC fields, which results in a decrease in the minimum operating pressure. For

example, a 13.56 MHz discharge can typically be sustained at a pressure of 0.5 Pa inside the vacuum chamber, while 9.0 Pa might be necessary with a DC field. The efficiency of the discharge, however, is not very high since during the positive cycle no sputtering of the target takes place.

3.1.6. Pulsed DC Plasma discharges.

A further increase in the efficiency of gas discharges (as compared to RF discharges) is achieved in the so-called pulsed DC discharge. In this case the polarity of the target is periodically switched from negative to positive for a short time interval as illustrated in Figure 10. This is particularly useful during the sputtering of metallic targets in a reactive atmosphere. The positive pulse is used to discharge the surface of the compounded target (since compounds normally are insulating) and thus avoid sparking and particle generation. The ratio between the duration of the positive and negative pulse is called duty cycle and is normally in the order of a few percent. Clearly, the efficiency of pulsed DC discharges is higher with respect to the RF counterpart since the effective duty cycle in the former is much smaller in addition to the steep transition between two polarities in the former case.
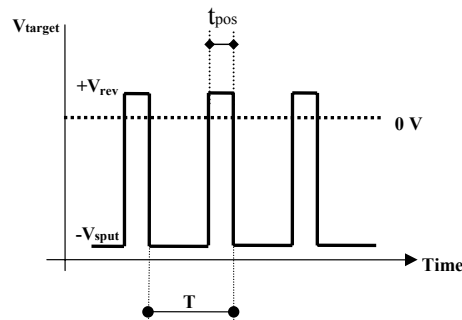
Figure 10 *Asymmetric bipolar pulsed DC*

It is noted that the amplitude of the positive pulse does not need to be large and is of the order of a few tens of volts. Very large amplitudes may result in undesirable effects such as sputtering the shields and chamber walls, leading to film contamination and damage. On the other hand sub-sputtering threshold amplitudes may give rise to beneficial mild ion bombardment of the growing film (normally below 50V).

3.2. Synthesis of AlN Thin Films

The main fabrication techniques for AlN thin films reported so far are thermal evaporation, chemical vapour deposition (CVD), reactive molecular beam epitaxy (RMBE) and reactive sputtering.

Epitaxial AlN films grown by chemical vapour deposition (CVD) on sapphire have been used to fabricate high frequency surface acoustic wave resonators and filters with near theoretical performance capabilities. However, the required substrate temperature of above 1000 °C is high and makes the process cost ineffective. The CVD technique is a commonly used method for the growth of III-V compounds owing to its excellent controllability and suitability for mass production. However, here again the high substrate temperature results in extensive grain growth giving rise to high surface roughness. This makes it difficult to fabricate a micropatterned (less than 1μm) interdigital transducer (IDT) on the AlN thin films without surface polishing. In addition, deposition of epitaxial AlN thin films on the basal plane [(001) Al_2O_3] or R plane [(112) Al_2O_3] sapphire requires temperatures higher than 500 °C.

Low-temperature growth of AlN thin films on silicon (Si) substrates is very important for the development of new hybrid optical integrated circuit (OIC). Among the techniques mentioned above, reactive sputtering at low temperature has the merits of simple and inexpensive fabrication for high quality polycrystalline films. This method can produce highly oriented fine grain polycrystalline films. To prepare AlN thin films with a high quality by the reactive sputtering method, a systematic study is, however, needed. It has been show that the AlN thin film surface deposited by low-temperature reactive sputtering is smoother than that of the AlN film deposited by the general MOCVD method. An IDT having a pattern size of less than 1μm can be fabricated on an AlN surface without surface polishing.

The better the orientation of the AlN films the stronger the SAW response, and the lower the propagation losses are. The acoustic properties of fine grain sputtered polycrystalline AlN films can reach the same acoustic performance level as that of single crystal epitaxial films.

3.2.1. Nucleation and growth of thin films

Depending on the short and long range ordering of the atoms in the lattice, materials are classified into three different categories, amorphous, single crystalline, and polycrystalline respectively. We focus our attention on the latter.

Polycrystalline thin films are primarily characterized by the size of the crystallites (grain size), their preferred orientation direction (texture) and the density. They are normally divided into the following three categories:

- Non-textured polycrystalline films: The crystallites are randomly oriented and hence all allowed reflections would be visible in the Θ-2Θ scan (see section 3.4.1).
- Textured: have a preferred orientation, which means that many crystallites grow in a specific direction but no epitaxial relationship exist between the film and the substrate.
- Epitaxial polycrystalline films: An epitaxial film is here defined as a polycrystalline film where the crystallites have specific in-plane orientational relationships with the substrate surface

The properties of a polycrystalline thin film may be quite different from those of the bulk, particularly if the film thickness is very small. These "anomalous" properties are due to the peculiar structure of the film, and the processes, which occur during film formation, in turn, dictate this structure.

Pashley et al.[52] distinguish four stages of the growth process: nucleation and island structure, coalescence of islands, channel formation, and formation of the continuous film.

Initially, the impinging flux of film species is thermally accommodated with the substrate after landing on the surface. After impingement, the species can both adsorb and stick permanently to the substrate surface atoms, they can diffuse on the surface (if they have sufficient energy) and interact with other adsorbed atoms ("**adatoms**"), or they can immediately be re-emitted (reevaporated).

Condensation is initiated by the formation of small clusters through combination of several adsorbed atoms. These clusters are called **nuclei**, and the process of cluster formation is called **nucleation**. Before the nuclei start to form island growth, in an attempt to decrease the total free energy of the system, they have to reach a **critical nuclei size**. The size of the critical nucleus is independent of the ability of single atoms to diffuse on the substrate surface. However, the rate of formation of critical nuclei clearly must depend on the ability of adsorbed atoms to diffuse and collide with each other. In essence, nucleation theory states that there will be a **barrier** to the condensation of permanent nuclei, determined mainly by the surface diffusion and the binding energy. If the activation energy for **surface diffusion** of adatoms at the substrate surface is very large, the diffusion distance before reevaporation will be small, and nuclei can grow only from material received by direct impingement from the vapour phase. The stronger the **binding energy** between adsorbed atoms and substrate, the smaller the critical nucleus and the higher the nucleation frequency. If a substrate is not homogeneous

but has sites of variable binding energy for adsorbed atoms, smaller critical nuclei are formed at tight binding sites, but at higher nucleation rates than at the weaker binding sites. A step on a substrate is an often-observed strong binding site.

If there is a large nucleation barrier (large critical nucleus with a high free energy of formation), the film will show an island structure in the initial stages of growth. This is known as the **island stage.** After an average thickness of a few monolayers has been deposited, under the regime of a large nucleation barrier, the film would consist of only a few, but large, aggregates. Under the regime of a small nucleation barrier the film will consist of many small aggregates, since the minimum stable size is now small, but the nucleation frequency is large. A film consisting of a dense population of small islands will become continuous at a relatively low average film thickness since these islands touch and grow together quite early in the deposition process. On the other hand, a film consisting of only a few big islands will have an island structure, which persists up to relatively high average film thickness. When the islands have joined together to form the grains of a continuous film, the effect of nucleation is often still visible: high-nucleation barrier films will give a coarse-grained film, while low-nucleation barrier films will give a finer-grained films (it should be noted here, however, that a single grain is generally formed by the coalescence of many nuclei).

Different nucleation barriers can therefore cause drastically different structures in thin films, but even the structure of a thick film can be at least partially traced back to nucleation phenomena.

Eventually these islands coalesce to form a continuous film, but this will generally occur only after the average film thickness has grown to several monolayers. In the **coalescence stage**, nuclei having well-defined crystallographic shapes before coalescence become rounded during the event.

The process of enlargement of the nuclei to finally form a coherent film is termed growth. Frequently both nucleation and growth occur simultaneously during film formation. Rather, there will be sufficient surface mobility on the substrate to lead to the formation of well-defined islands of film material on the substrate even long after the nucleation step.

In the **channel stage**, the islands become elongated and join to form a continuous network structure in which the deposit material is separated by long, irregular, and narrow channels of width 50 to 200 Å.

During the formation of the **continuous film**, considerable changes in the orientation of islands occur during the growth of the film, particularly in the coalescence stage. Some recrystallization occurs during coalescence, so that the grain size of the completed deposit film is large compared with the average separation of the initial nuclei. Thus, the grain size of the completed film is controlled by the recrystallization, which occurs during coalescence of nuclei or islands, not only the initial density of nuclei.

3.2.2. Reactive sputtering

The impact of an energetic atom or ion on a surface produces sputtering from the surface as a result of the momentum transfer between the incident particle and the target atoms. Unlike many other vapour phase techniques there is no melting of the material. The verb SPUTTER originates from Latin SPUTARE (To emit saliva with noise). This phenomenon was first described 150 years. Grove (1852) and Plücker (1858) first reported vaporization and film formation of metal films by sputtering. The key for understanding this process was the discovery of electrons and positive ions in low-pressure gas discharges (J.J. Thomson) and atom structure by Rutherford, at the end of the last century.

Reactive sputtering is a process where a metallic target is sputtered in a reactive atmosphere as illustrated in Figure 11, which for specificity shows the sputtering of Al in an Ar/N_2 ambient for AlN deposition.
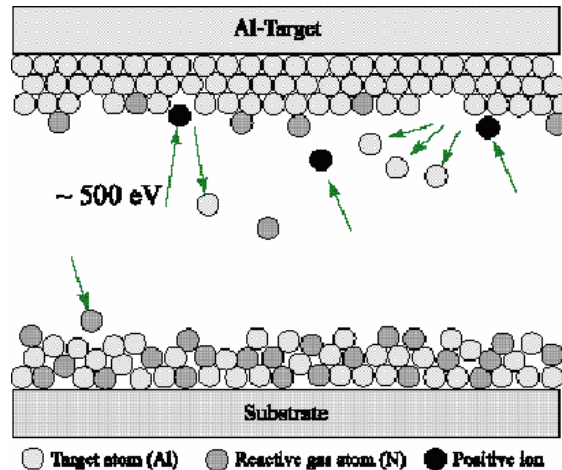
Figure 11 *An illustration of the reactive sputter process, where in this case the aluminium reacts with the nitrogen to form aluminium nitride.*

As the sputtered atoms are deposited onto the substrate they react with the reactive gas molecules (N_2 in this case) forming thereby the desired compound.

Reactive sputtering has some important advantages as compared to sputtering from a compound target:

- Metal targets can easily be machined and are cheaper.
- Metal targets have high thermal conductivity enabling efficient target cooling and hence the possibility to apply a substantially higher power, e.g. 50 W/cm^2, without melting the target.
- By employing certain tailored process techniques, high rates comparable to those of pure metals can be obtained.

- A particular metal can be utilized for the synthesis of several different compounds, offering good process versatility.

There are also certain disadvantages associated with reactive sputtering. The process is extremely complex, and in order to obtain desirable results, process understanding and optimization of all the parameters influencing film quality is required. Simulation of the reactive sputtering process can readily be performed using the model developed by Berg et al[53, 54]. To get a better insight into the process it is instructive to take a look at its behavior as a function of the major process parameters. Although, the discussion below is generally valid for any reactive sputter deposition process, for clarity, we often refer to the case of AlN.

A. PROCESS PRESSURE

According to the kinetic theory of molecular gases, the mean free path of a gas molecule at constant temperature has a value that is inversely proportional to the pressure. At low sputtering pressures, the mean free paths of the species increases owing to the decrease of the particle scattering, and the energetic particles in the plasma can easily transfer their kinetic energy to the adatoms at the growing film surface. This effect namely the kinetic energy of the sputtered atoms is utilized in Paper IV to promote growth of highly c-axis oriented AlN films at room temperature[55]. Another widely observed effect at low pressures is the bombardment of the growing film with fast neutrals, i.e. energetic ions that are reflected and neutralized upon impact with the target. The energy of fast neutrals is sufficiently high to cause re-sputtering[56, 57] and damage in the growing film.

Generally, the c-axis orientation of the film changes from perpendicular to parallel with respect to substrate surface as the sputtering pressure increases. The basal plane in the hexagonal structure has the lowest surface energy and the maximum atomic density and hence, the c-axis orientation improves due to the increase of kinetic energy transfer at the film surface as the sputtering pressure decreases.

Normally, the magnitude of compressive stress increases drastically with decreasing sputtering pressure. This can be understood in terms of internal stress accumulation by relatively high momentum transfer at the film surface at low sputtering pressures. Atomic bombardment at the film surface results in compressive stress in the film and film densification by decreasing the voided regions in the microstructure (see Paper V for further details).

B. (Ar/N$_2$) FLOW RATIO

The addition of an inert component to the gas mixture offers a number of advantages. It may increase the sputtering yield and hence the deposition rate. In addition, it provides an easy way to control the flux and type of both gas molecules and ions arriving at the film surface. In other words, varying the gas composition provides a means to control both film stoichiometry and structure.

As the nitrogen concentration increases while the sputtering pressure is kept constant, the increase of c-axis orientation of deposited film is attributed to the change of chemical species in the plasma, since the values of the mean free paths

of N_2 and Ar are approximately the same. Besides, the full width of half maximum intensity (FWHM) of the AlN (002) peak decreases with increasing N_2 concentration, that is, the crystallization of AlN thin films is improved.

The Ar/N_2 ratio affects also the residual stress of the films as discussed in Paper V.

C. DISCHARGE POWER

The discharge power affects the growing film in several ways. Firstly, a relatively high deposition rate reduces the impurity incorporation into the film from background gases. On the other hand, high deposition rates result in a decrease in the ion/atom flux ratio at the substrate during ion assisted deposition resulting in worsened texture as well as tensile stress. Finally, extremely high deposition rates may result in nonstoichiometric films as well as structural defects due to reaction and diffusion limitations. Low deposition rates on the other hand result in poor film quality mainly due to background gas incorporation.

D. SUBSTRATE BIAS

A negative bias is normally applied to the substrate to achieve ion assisted deposition, that is, the ions are accelerated by the applied bias and bombard the growing film. This brings about a number of beneficial effects as follows. For moderate bias values, say below 50V, the ion bombardment deposits kinetic energy at the surface of the growing film, enhancing thus surface diffusion and hence film texture and surface smoothness. In addition, the enhanced diffusion results in denser films, that is changes the stress from tensile to compressive. All this has the effect of stimulating crystal growth at low temperatures, which is one of the greatest advantages of plasma PVD deposition processes. An important quantity in ion assisted deposition is the ion/atom arrival flux ratio F, which defines the relative energy deposited by the ions per one deposited atom. The higher this energy is the better the quality of the films. On the other hand, high bias values generally result in resputtering and most importantly to damage production and even amorphization of the film. For this reason, the energy of the ions is kept below a critical value and hence the deposited energy is only controlled by the ion/atom arrival ratio F, which requires denser plasmas.

E. SUBSTRATE TEMPERATURE

The growth temperature is perhaps the most effective crystal growth promoting process parameter. In practice, however, it is often desirable to reduce the temperature as much as possible. Thus, high deposition temperature increases the cost of the process, introduces thermal stresses, increases impurity incorporation, etc. These are very important issues in device fabrication, for which reason a substantial effort has been made in this work to reduce the process temperature.

3.3. Lithography and Etching

Most of the processing steps here are borrowed from the standard IC fabrication technology and are hence omitted in this discussion. It is only noted that in view of the fabrication of thin film electroacoustic devices a few etch processes need to be developed. Thus, for SAW devices Al electrodes have to be defined on top of the AlN film, which requires a highly selective etch process of Al with respect to AlN. In addition, the etch process has to be highly anisotropic since control over the line definition (electrode profile and width) is essential for high performance SAW devices. These issues have been addressed in Paper III in this work. For BAW devices a contact hole needs to be opened through the AlN layer to contact the bottom electrode, which requires a proper choice of bottom electrode material. Thus the latter has to have both excellent electrical and acoustic properties as well as very good selectivity with respect to the AlN etch process. All these issues have been addressed in this thesis.

3.4. Analytical techniques

3.4.1. X-ray Diffraction

X-ray diffraction (XRD) is a powerful analytical method for determining the structural properties of materials, such as crystal structure and orientation, lattice parameters, film texture and thickness, grain size and orientation, stress, etc. This is achieved by using the method in a variety of modes. The most widely used ones are as follows.

a) Θ -2Θ Scan

In this type of scan, the incident angle ω and the reflected angle Θ are equal. The x-ray source and the x-ray detector are coupled during the scan. From the XRD diffractogram one readily extracts the lattice parameter, film texture, grain size, etc.

b) Rocking Curve

The sample is rotated (rocked) through an angular range, bringing the plane in and out of the Bragg condition. The width of the measured peak, normally measured in terms of the Full-Width at Half Maximum (FWHM) value contains information of the amount by which the measured plane is off the surface normal, sometimes referred to as the "degree of orientation" of the specimen. This method enables also accurate determination of very small deviations in d-spacing due to strain effects etc and is widely used to compare the crystalline quality of thin films.

c) Φ-Scan

A Φ-scan measurement[58] is performed by studying two crystallographic planes, one from the substrate and one from the film which are not parallel with the sample surface. The incident X-ray is locked at an angle ω defined by the chosen plane and the detector is locked at the diffraction angle 2Θ for the same plane. The Φ-scan is then performed by rotating the sample around its normal while the intensity of the plane is simultaneously recorded. The in-plane orientational relationship can then be determined by comparing the positions of the resulting peaks from the two Φ-scans.

3.4.2. Atomic Force Microscopy (AFM)

The atomic force microscopy (AFM) probes the surface of a sample with a sharp tip, a couple of microns long and often less than 100 Å in diameter. The tip is mounted on a flexible cantilever that is 100 to 200μm long. Forces between the tip and the sample surface cause the cantilever to bend and a laser diode reflecting the signal back to a photodetector CCD array is used to sense the movement. Precise control of the tip movement over the surface to be scanned is made by the use of piezoelectric ceramics.

Atomic force microscopy (AFM) has become a very powerful analytical technique in materials science since this measurement can give information on surface morphology on a nanometer scale without vacuum isolation.

3.4.3. Scanning Electron Microscopy (SEM)

Secondary electron microscopy, SEM, is used to examine physical features with dimensions from several microns down to a few nanometers. Secondary electrons emitted/scattered from the surface are detected in synchronization with the raster. The orientation of surface features influences the number of electrons that reach the secondary electron detector, which creates variations in image contrast that represent the sample's surface topography. The secondary electron image resolution for an ideal sample is about 3 nm making it suitable for topographical and morphological analysis of materials. Thus, this method provides high-resolution imaging of fine surface morphology.

3.4.4. Transmission Electron Microscopy (TEM)

TEM microscopy uses a focused beam of energetic electrons shone onto a very thin specimen. The transmitted beam is then projected onto a screen. TEM provides morphology and crystallographic information such as the size, shape and arrangement of the constituents of the specimen as well as their relationship to each other (misalignment, defects etc) on the atomic scale. Specimen for TEM analysis must be specially prepared to thicknesses, which allow electrons to transmit through the sample. Because the wavelength of electrons is much smaller than that of light, the optimal resolution attainable for TEM images is many orders of magnitude better than that of a light microscope. Thus, TEMs can reveal the finest details of internal structure - in some cases as small as individual atoms. Magnifications of 350,000 times can be routinely obtained for many materials. In special circumstances, atoms can be imaged at magnifications greater than 15 million times.
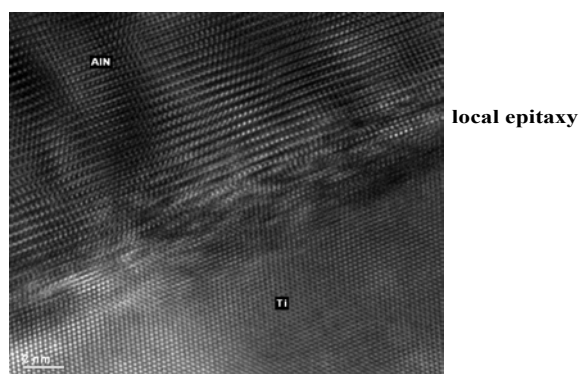
Figure 12 *TEM image of (0002) AlN on (0002)-Ti substrate. The individual atoms on both layers can be appreciated. The pictures show local epitaxy of the AlN layer on the Ti substrate.*

3.4.5. Electron Spectroscopy for Chemical Analysis (ESCA)

Electron spectroscopy for chemical analysis (ESCA, also known as X-ray photoelectron spectroscopy or XPS) exploits the photoelectric effect to obtain information about the chemical composition and structure of a surface. It is an absolute method (no calibration standards are needed) with a resolution of around 0.5 %. It is also a surface technique, but combined with ion beam sputtering can be used for depth profiling.

4. Summary of Papers

Paper I

In this paper, the deposition of polycrystalline AlN thin films on thermally grown SiO_2 using RF reactive sputtering has been systematically studied. The films have been optimised with respect to RF power, Ar/N_2 ratio, process pressure, and substrate temperature. The properties of interest are crystallinity, degree of orientation, crystallite size, surface roughness, stress, piezoelectric coupling, acoustic velocity and others. It is found that these properties are all very sensitive to the deposition parameters. The films have been analysed with RBS, ESCA, XRD, ellipsometry, SEM, AFM, stress measurements, etc. Films deposited at optimal deposition parameters were shown to be of very high quality with the c-axis perpendicular to the substrate surface.

a) Stoichiometry

Initial deposition experiments were done on carbon substrates and analysed with RBS to determine stoichiometry and deposition rate as a function of gas composition. It was found that stoichiometric films were grown for N_2 to Ar ratio greater than 1. One of the most important impurities in the films was found to be oxygen. As the affinity of oxygen towards Al is much higher than that of nitrogen, almost all oxygen from background gases is incorporated into the films. Oxygen has been found to be detrimental to the piezoelectric properties of AlN, and care must be taken to eliminate it as much as possible. Impurity levels were monitored by ESCA analysis. Figure 13 shows a typical ESCA spectrum of a thin polycrystalline AlN film. As seen the only detectable impurity is oxygen and its content has been found to be about 0.5%.
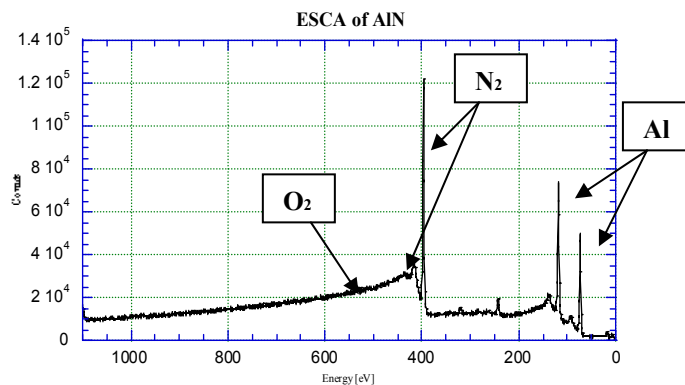

Figure 13 *ESCA graph of highly oriented AlN deposited on (111)-Si by the reactive sputtering method.*

b) Structure

The structural properties are of great importance since they determine the piezoelectric properties of the films. As the (0002) plane is the fastest growing plane, nonepitaxial polycrystalline films normally exhibit a preferred growth in the (0002) direction. The degree of orientation is then measured by the presence of peaks other than (0002) and its multiples. The most frequently observed non (0002) peaks are (100), (101), (102), and (103). The quality of the (0002) films is inversely proportional to the intensity of these peaks. In most publications the XRD spectra are presented in a linear scale, which can be misleading since the large intensity of the (0002) peak can disguise the much smaller (100) to (103) peaks. For this purpose XRD spectra here are presented in a log scale. Further, to make the spectra comparable to each other the thickness of the AlN films was kept constant (1 micron) for all deposition conditions. The structural properties of the films are considered as most important with respect to obtaining films with high piezoelectric constant, low propagation losses, etc. Cone orientation and tilt, cone size, density, surface roughness, are among others the parameters optimised in this work by varying the deposition conditions.

Further, to study the electroacoustic properties of the films, thin film transversal test structures consisting of non-apodized Al interdigital transducers formed on AlN/SiO$_2$/Si were fabricated and evaluated with a network analyser. The measurements indicated a SAW velocity of 4900 m/s, propagation losses of 4.7 dB/cm and an electromechanical coupling of 0.37%. Figure 14 shows the frequency response of a SAW filter with a center frequency of 0.548 GHz filter formed on AlN/SiO$_2$/Si.
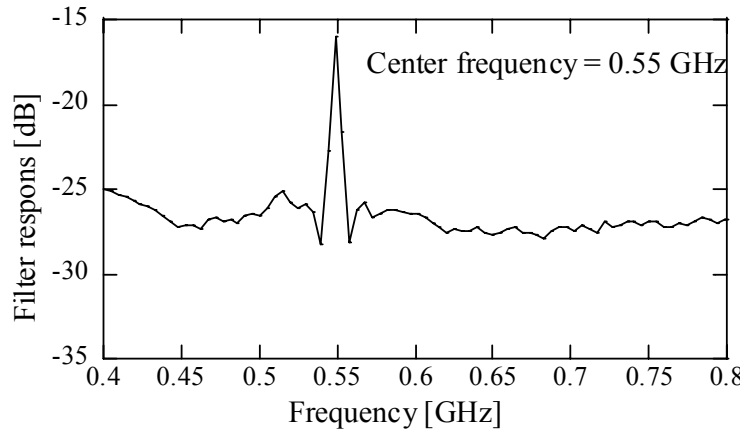

Figure 14 *Frequency response of a SAW filter formed on AlN/SiO$_2$/Si.*

Paper II

In this Paper, AlN thin films were deposited on several different substrates by using radio frequency (RF) reactive sputtering in an Ar/N_2 ambient. In addition to films deposited on thermally grown SiO_2, growth of highly oriented AlN films has also been studied on a number of polycrystalline (Al and Pt) and monocrystalline (Si and $(001)\alpha-Al_2O_3$) materials. Al and Pt are suitable materials for bottom electrodes in BAW devices while sapphire is used as a reference substrate to compare film properties with epitaxial AlN films[59, 60].

The structural properties of the films were optimized by systematically varying deposition parameters such as process pressure, gas mixture, substrate temperature, and discharge power. It was found that all the substrates used in this investigation resulted in films of very high quality with a complete (002)-orientation, provided that the substrate surface was sufficiently smooth. The films deposited on sapphire were epitaxial despite the relatively low deposition temperature of 500°C, and showed a FWHM of the (002) rocking curve of 0.4°. The surface of the grown films was very smooth in the same range as a polished silicon surface. This result is also confirmed in Paper VII and indicates a high surface mobility of the atoms during film growth.

Further, AlN films have also been grown on $(001)\alpha-Al_2O_3$ for comparative reasons. XRD studies show that the films are epitaxial. To achieve epitaxial growth, however, the deposition temperature had to be increased to 500°C. In-plane epitaxy was determined from ϕ-scans of the 202 peaks with the ϕ-rotation axis parallel to the c-axis of the films. Figure 15 shows ϕ-scans of both the AlN film and $\alpha-Al_2O_3$. For the AlN 202 peaks a separation of 60° was observed, revealing the six-fold symmetry of the AlN(001) surface. The $\alpha-Al_2O_3$ {202} plane has also a 6-fold rotational symmetry and all these peaks should be visible with a ϕ-scan around the (001) plane at $\chi= 72.4°$. However, only three peaks with a separation of 120° are visible on the ϕ-scan. This can be explained by the extinction of the (20-2), (-202) and (022) planes yielding peaks from only the (202), (02-2) and (0-2,2) planes. The peak positions of AlN(202) with respect of the Al_2O_3(202) peaks indicate that the lattice of the AlN film is rotated 30° relative to that of the $(001)\alpha-Al_2O_3$ surface to minimize lattice mismatch. A rotation of 30° corresponds to an in-plane epitaxial relationship of: [100] AlN//[120] $\alpha-Al_2O_3$**.** The ϕ-scan peaks are relatively broad with FWHM values of about 1.5-1.6°, indicating an in-plane domain structure.
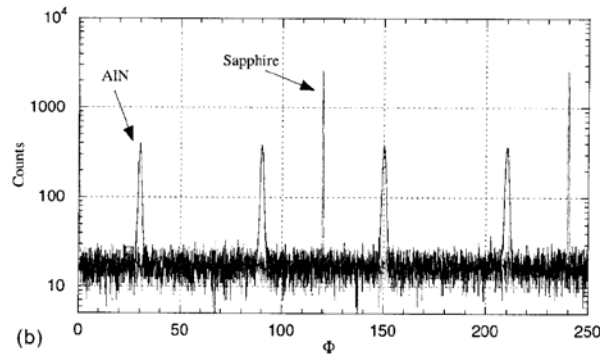
Figure 15 *XRD ϕ-scan of AlN grown on (00l)α-Al₂O₃.*

The rocking curve value of the 002 peak for films deposited at 500°C is found to be 0.4 degrees, which is rather good considering the relatively low deposition temperature. The rocking curve value indicates a relatively good alignment of the c-axis with the substrate (001) plane and a low defect density. This is the lowest reported rocking curve FWHM value at a temperature under 500°C to our knowledge.

Paper III

Metallization is a very critical step in the fabrication of high frequency Al/AlN/Substrate thin film based surface acoustic wave devices. The AlN surface in such applications is extremely sensitive to both particles from the lithography, as well as ion induced damage from the etch process. In this Paper, etching characteristics such as etch rate and selectivity between the materials of interest was studied using an Inductively Coupled Plasma (ICP) etching system. The goal was to find a recipe that etches Al at a sufficiently high rate, while having at the same time a very high selectivity with respect to the underlying AlN film. The starting point was a Cl based chemistry with the addition of O_2 to slow down the lateral etch component. The dominant etch mechanism for the removal of Al was found to be ion assisted chemical etching, whereas the main mechanisms for the AlN etch was predominantly physical sputtering. Thus, process parameters resulting in a very high selectivity (typically 1000) between Al and AlN could be found by keeping the applied bias at a sufficiently low value. At the same time, very high Al etch rates of the order of 1μm/min have been achieved. Hence, Al/AlN/Substrate structures with perfect Al pattern delineation and an intact AlN surface could be realized. The etch rate of Al was typical 1 micron/minute, which is very high indeed.

In addition to high selectivity and etch rates exact pattern transfer, that is, obtaining vertical sidewalls is essential for the fabrication of SAW devices. This in turn is governed by the anisotropy of the process. Thus, it is mandatory that the lateral etch rate of Al is practically zero. Without the addition of oxygen the etch process is almost completely isotropic as seen from Figure 16 which represents a cross-sectional SEM micrograph of an Al line etched under the following conditions: 500 W ICP power, 83 V bias, 50 sccm BCl_3, 25 sccm Cl_2, 0 sccm O_2, 0 sccm Ar and a pressure of 10 mTorr.
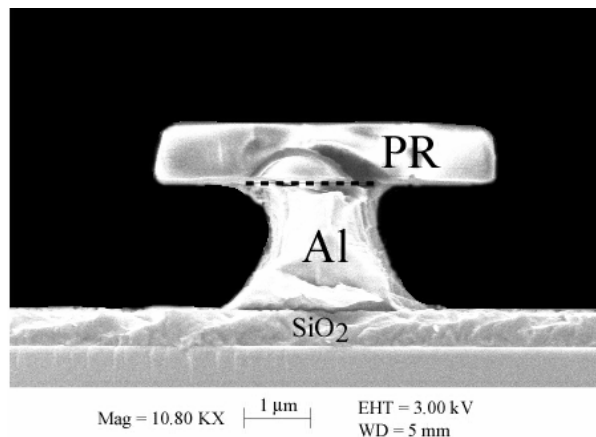
Figure 16 *SEM micrograph of an Al line etched without oxygen addition.*

It is seen that the underetch is considerable resulting in a substantial loss of resolution. This, as argued above, is to be expected since the etch mechanism of Al is predominantly chemical, which generally is independent of the etch direction.

In contrast, the addition of small amounts of oxygen results in oxidation of the Al surface. This oxide is consequently sputter-removed from the areas exposed to the ion bombardment from the plasma, i.e. the bottom of the trenches. Note that the ion bombardment generally is directional, that is, normal to the surface although with a certain divergence. On the other hand, the Al oxide on the sidewalls under the mask is shadowed from the ion bombardment and hence the lateral etching of Al is completely blocked. This wall passivation results in a highly anisotropic process as seen from Figure 17.
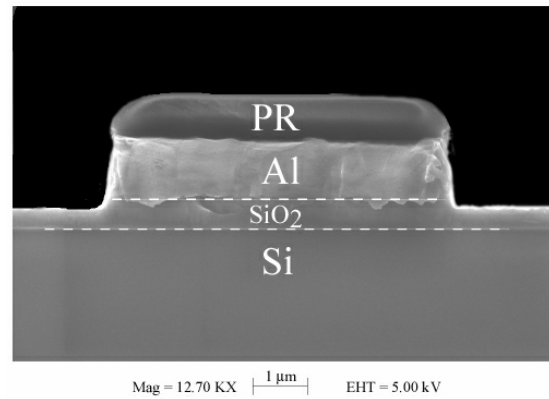

Figure 17 *SEM micrograph of an Al line etched with oxygen added to the plasma.*

The latter represents a cross-sectional SEM micrograph of an Al line etched under the following conditions: 500 W ICP power, 83 V bias, 50 sccm BCl_3, 25 sccm Cl_2, 10 sccm O_2, 0 sccm Ar, pressure 10 mTorr. It is seen that the pattern transfer in this case is exact as long as the mask does not start receding laterally. It is noted that the Al has been deliberately and substantially overetched to demonstrate that no loss of resolution occurs even at long overetch times.

Paper IV

The deposition temperature of a specific film is very important in IC-fabrication, particularly for back end processes, since high temperatures may affect the rest of the device in an undesirable and sometimes detrimental way. One of the most likely ways for integrating the thin film electroacoustic technology with the IC-technology is back end integration, which by obvious reasons allows a rather low thermal budget for the electroacoustic component. This necessitates the development of low temperature deposition processes of the piezoelectric film, which is the main focus of this paper, namely low temperature synthesis of highly textured AlN thin films with pulsed DC reactive sputtering. To achieve this we studied systematically the influence of the major process parameters on the film texture. It was found that the process pressure had a profound effect on the film texture as it determines the deposition rate, the energy and direction of the condensing Al atoms, the impurity incorporation into the film, and hence influences significantly the film properties. It was found that at pressures below 2 mTorr, the films had an excellent (002) orientation as well as very good electroacoustic properties and could be synthesized at room temperature.

Our explanation for the drastic improvement in film orientation at low pressures leads to a different energy delivering mechanism named by the authors as "atom assisted growth" (AAD). It is well known that the energy of the sputtered atoms is distributed as shown in Figure 18, where Us/2 is half the surface binding energy of the sputtered atoms. This energy, typically of a few (1 to 4) electronvolts for most metals, is high enough to promote crystal growth, but not to induce damage at the substrate surface. Using atom-assisted growth, the atoms are allowed to reach the surface with a sufficient fraction of this energy, which is made possible by sputtering at very low process pressures.
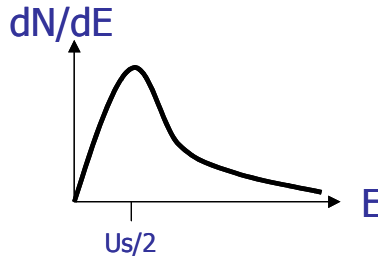

Figure 18 *Energy distribution of sputtered atoms.*

From basic kinetic theory, it can be shown that the mean free path of the atoms in the gas phase is a function of the pressure P and is given by

$$(39) \qquad \lambda_{mfp} = \frac{5}{P} \frac{[\text{mTorr} \quad \text{cm}]}{[\text{mTorr}]}$$

From Eq. (39) we see that the mean free path of atoms sputtered at 10 mTorr is around 0.5 cm. However, the mean free path when processing at 1mTorr is approximately 5 cm. This mean free path is close to the Target to Substrate distance in the sputtering system used. Hence, when sputtering at low process pressures (< 2 mTorr) the atoms do not loose their original energy by collisions in the gas phase. They are allowed to reach the substrate in a collision free path and are hence high energetic as they arrive at the surface. As a consequence of that, the species that need to surface diffuse are themselves high energetic and no external stimulation is needed. Moreover, the atoms themselves deliver energy at the surface and help other atoms and clusters to surface diffuse, hence improving the adatom mobility.

Figure 19 shows the X-ray diffraction Θ-2Θ scans of AlN films deposited on Si as a function of the process pressure.
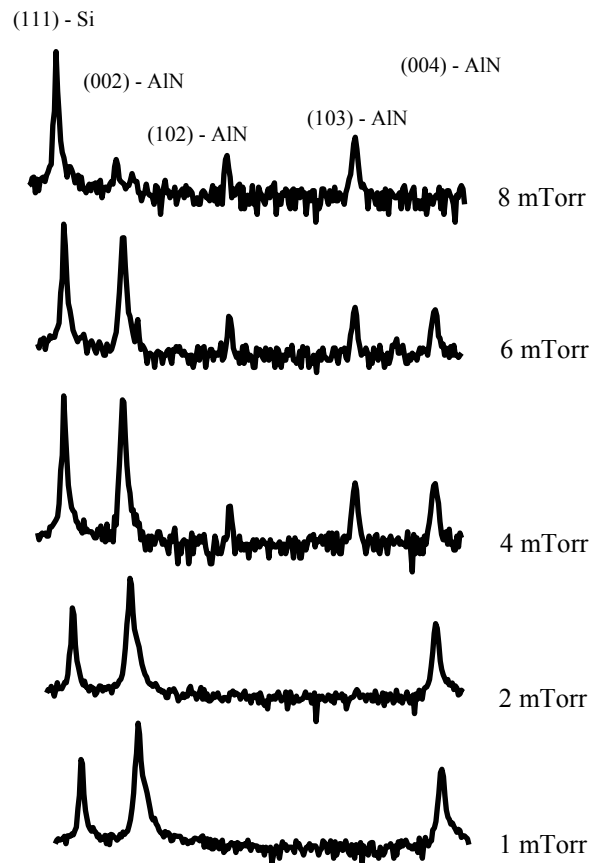
Figure 19 *Θ-2Θ scan of AlN films as a function of the process pressure.*

Looking at the first film, deposited at a high process pressure of 8 mTorr, we see a polycrystalline film where different orientations (102), (103), (002) and its derivative (004) appear. No preferred orientation can be determined in this film. Lowering the pressure to 6 mTorr, the (002)-peak becomes dominant, but other orientations are still present, which indicates a poorly oriented film. In the film deposited at 4 mTorr, although not easily seeing in the picture in spite of the logarithmic scale used, the intensity of the 002-peak is higher as compared to the 6mTorr-film, and the intensities of the (102) and (103) peaks are lower, but still apparent. However, the Θ-2Θ scans of the two films in the lower part of the picture, deposited at process pressures of 2mTorr and 1mTorr respectively, show a typical Θ-2Θ scan of a highly c-axis oriented AlN film, where only the 002-peak and its derivative, the 004-peak are visible. Since all other process parameters were the same in each experiment, we conclude that the process pressure can be regarded as the only parameter responsible for the dramatic improvement in the texture of the AlN-films.

Thus using AAD, films with (0002) FWHM rocking curve values of around 1.8° have been routinely grown on (111) Si substrates at room temperature, which is an extremely good result. Just as a reference, it has been found that films with (0002) FWHM rocking curve values under 3° suffice for the industrial fabrication of electroacoustic devices, since the electromechanical coupling remains fairly constant for such films. Of course, using in addition thermal stimulation improves further the texture of the film. Thus, we have found that films grown at 300°C exhibit on average (0002) FWHM rocking curve values of around 1.6°.

Paper V

The very high residual stress often observed in polycrystalline A1N thin films often results in both performance deterioration of electro-acoustic devices as well as decreased lifetime (component failure). Substrate deformation and distortion necessarily arise from stresses in the overlying films. In integrated circuit technology even a slight bowing of silicon wafers may result in significant problems with regard to maintaining precise tolerances in pattern delineation. Compressive stresses produce a convex curvature (negative radius) in the silicon substrate and are hence given as negative values whereas tensile stresses lead to a concave curvature (positive radius), which explains the positive values used to represent them. In this work, the magnitude of the stress evolution in fully textured AlN films was systematically studied as a function of the main process parameters during reactive sputter deposition. The stress was evaluated from the change in the radius of substrate curvature before and after deposition. It is found that all the major deposition parameters, such as process pressure, gas flow, substrate bias, and discharge power affect substantially the residual stress in the films. It is also argued that the major mechanism responsible for stress evolution in the films are atom assisted deposition and atomic peening. It is shown that the stresses can be controlled by the deposition parameters, and that stress free films can be deposited at room temperature at optimized conditions. Figure 20 shows the typical behavior of stress as a function of the amount of Argon in the gas mixture. In this work, it was found that all major process parameters mentioned above exhibit a similar behavior.
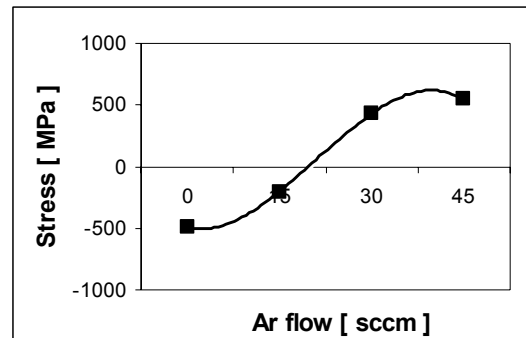

Figure 20 *Residual stress as a function of the Argon content in the gas mixture*

Paper VI

In this paper, both MIS and MIM structures based on amorphous and polycrystalline reactively sputtered AlN films have been electrically evaluated. The polycrystalline films were highly (002) oriented with the c-axis perpendicular to the substrate surface. CV measurements revealed a very stable dielectric constant of 10 regardless of the crystallinity of the film (including amorphous). Additional dielectric measurements using a network analyzer showed that the dielectric constant was also very stable with frequency up to 10 GHz. High frequency measurements were made on MIM structures using Mo as the bottom electrode. The interfacial layer between the Mo and the AlN is, using the same procedure as in the MIS case, estimated to be 15 Å. It is seen that the capacitance remains constant in the measured range, and scales with both the dielectric film thickness and the area of the active device.

Leakage currents through the AlN film were found to be Poole-Frenkel controlled, and hence thermally activated. The properties of the AlN as determined from these studies indicated that the material is very promising for integrated capacitors and possibly as a gate dielectric.

The dielectric loss function, tan δ, defined as the imaginary part of the dielectric constant divided by the real part, is shown in Figure 21. The signal is somewhat noisy, although it stays relatively constant at a value below 0.03 in the measured frequency range. The noisy behavior of the dielectric loss in Figure 21 is believed to be due to problems associated with contacting the bottom electrode of the structures.
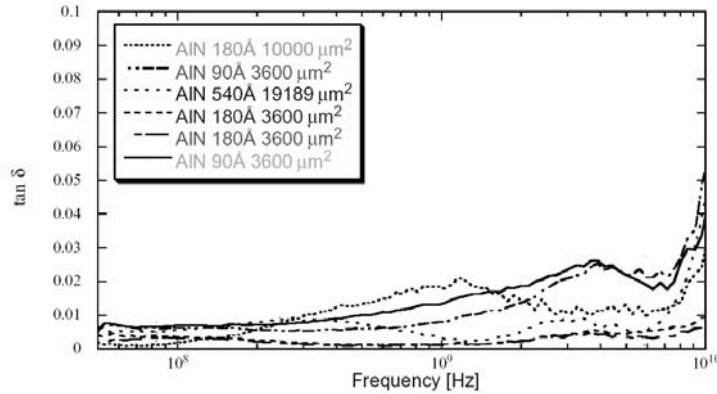

Figure 21 *The dielectric loss tangent for different areas and different film thicknesses.*

Paper VII

Thin piezoelectric polycrystalline films such as AlN are of great interest for the fabrication of Thin Film Bulk/Surface Acoustic Resonators (TFBAR) or (TFSAR). Thin metal layers are used to form the bottom electrode of TFBAR as well as to define a short-circuiting plane in TFSAR devices. In both cases, they serve as a substrate for the growth of the piezoelectric film. It is well known that the degree of c-axis orientation of the thin films correlates directly with the electro-mechanical coupling. The texture of the piezoelectric films in turn is influenced by the structure of the substrate material.

This work focuses on the growth of highly c-axis oriented thin AlN films on Mo, Ti, Al, Ni and TiN layers. These materials have been chosen for different reasons in this study. Thus, Al and Mo have low resistivity and high Q factors. Ti has a hexagonal structure similar to that of AlN, while TiN is a nonmetallic conducting material. Ni was chosen for its good surface smoothness. Other factors include etch selectivity of the bottom electrode with respect to the AlN film. The aim is to identify which factors and properties of the underlying material influence the texture of AlN and hence optimize both at the same time. The surface roughness as well as the degree of orientation of the five materials considered in this work has been systematically studied, in an attempt to understand how this factors affect the orientation of the AlN thin film deposited on them. It has been found that the texture of the bottom metal layer affects significantly the texture of the AlN films, and hence its electro-acoustic properties.

Figure 22 shows the degree of c-axis orientation of AlN thin films grown on high conducting layers synthesized at four different pressures.
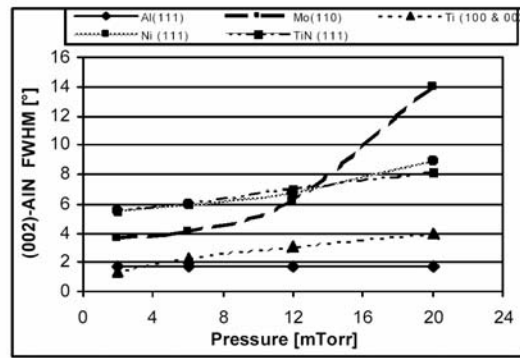

Figure 22 *Degree of crystallographic orientation (FWHM) of the 002-peak of AlN thin films grown on high conducting layers as a function of the deposition pressure of the latter. The deposition parameters of AlN were kept constant for all experimental points.*

The results from the above optimisation process have been used for the fabrication of FBAR resonators of membrane type. The latter were fabricated by bulk micromachining by etching the Si wafer from the backside. Both Al and Ti electrodes were used for comparison. In the case of FBAR with Al electrodes, the resonators consisted of 200 nm top and bottom electrodes and a 2 μ-meter thick AlN layer. For FBAR with Ti electrodes, the resonators consisted of 50 nm Al (necessary as an etch stop barrier) and 150nm Ti bottom electrodes and a 2 μ-meter thick AlN layer. The top electrode had a similar structure as the bottom electrode for symmetry reasons. The Equivalent Circuit Model (ECM) used to simulate the resonating BAW structure with Ti electrodes is shown in Figure 23.
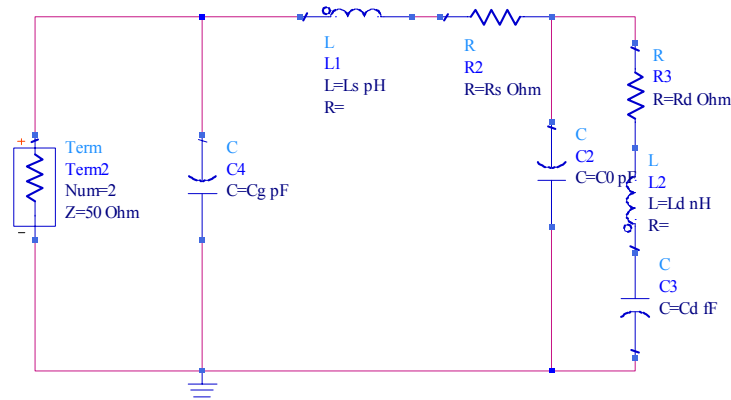
Figure 23 *Equivalent Circuit Model (ECM) used to simulate the resonating BAW structure with Ti electrodes*

The impedance characteristics of the resonator with Ti-electrodes as well as the fitted curves are shown in Figure 24 (fitted and measured curves are undistinguishable).
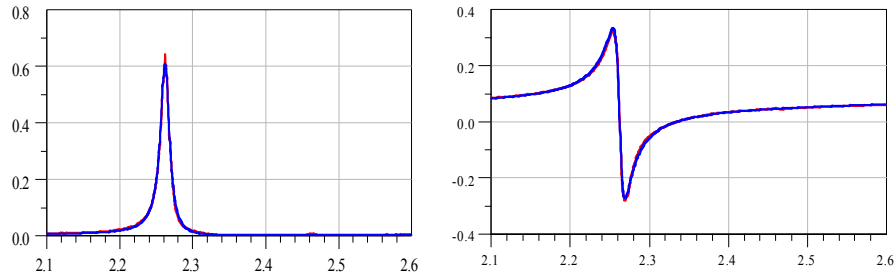

Figure 24 *Real part. (left) and Imaginary part (right) of the resonance peak of the FBAR resonator with Ti-electrodes.*

Both Al and Ti electrodes types of FBAR structures exhibited an electromechanical coupling coefficient k_t around 0.253, and a Q factor around 500. It is noted that the theoretical electromechanical coupling coefficient for single crystal AlN is $k_t = 0.255$.

Paper VIII

In this work, the properties of AlN thin films grown on diamond substrates at room temperature as well as the various SAW modes excited in the AlN/diamond structure have been studied.

The c-axis orientation of AlN deposited on diamond has not been optimised specifically due to shortage of substrates, but was nevertheless rather good. Thus the (0002) FWHM rocking curve values of the AlN films were of the order of 2.1° as shown in Figure 25.

Rocking curve of (002)-AlN peak

FWHM: 2.1°

Intensity (arb. units)

Degrees
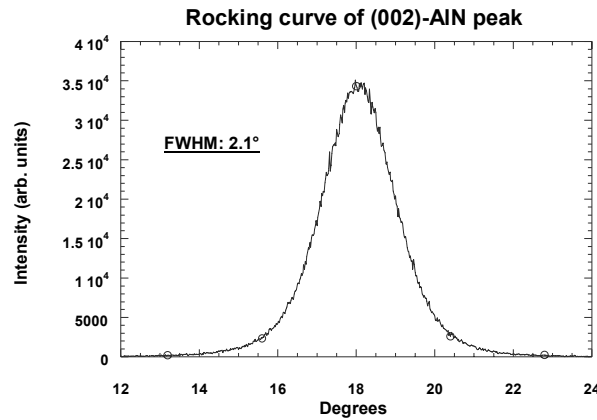
Figure 25 *Rocking curve of the (002)-peak of highly oriented AlN deposited on polished polycrystalline diamond substrates at room temperature.*

It is well known that any departure from the ideal crystal structure in acoustic propagation leads to increased acoustic losses. Hence, and particularly in the case of polycrystalline thin films grown at room temperature, it is important to determine the surface roughness of the AlN films, since large surface roughness may lead to increased scattering and hence increased propagation losses. Atomic Force Microscope (AFM) scans were performed on the AlN surface of the films synthesized on diamond substrates in order to study the influence of the growth conditions on the morphological properties of the thin film as well as to address their possible impact on the propagation of acoustic waves. Closer inspection of the AFM images reveals that the AlN surface is rather smooth with shallow groove-like features that run along grain boundaries of the polycrystalline diamond film (see paper for further details).

The dispersion of the phase velocity for the latter is shown in Figure 26 as a function of the normalized AlN film thickness, i.e. the ratio between the latter and the wavelength. The thickness of diamond (50μm) is assumed to be sufficiently large to neglect the effect of the silicon substrate beneath the diamond since the SAW energy is confined to a depth of maximum 2 wavelengths from the surface. The calculations are given for the Raleigh wave and its higher modes (Sezawa waves), which we call the 0-th mode, the 1st mode, the 2nd mode and the 3rd mode wave in the text and figures, hereafter. For all wave modes, an increase in the phase velocity with decreasing the A1N film thickness is observed which is expected since the relative contribution to the phase velocity from the diamond substrate increases accordingly.
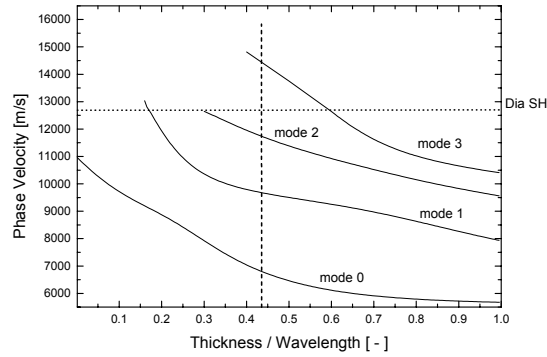
Figure 26 *Thin film thickness dependence of the phase velocity in the IDT/AlN/diamond structure*

Similarly, the dispersion of the coupling coefficients for IDT/AlN/diamond are shown in Figure 27. The latter shows that mode 1 exhibits a broad maximum. In other words, a coupling coefficient of the order of 1.2% can be achieved with a high phase velocity of 11090 m/s. Overall, the AlN/diamond system is suitable for mid-bandwidth applications in SAW devices.
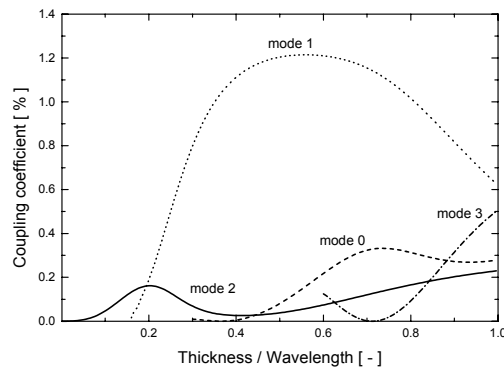
Figure 27 *Coupling coefficient of the IDT/AlN/diamond structure*

The S_{11} parameter of the fabricated resonators was measured in the frequency range from 500MHz to 2500MHz. The results obtained for a test structure with an aperture of 200 microns, 801 electrodes in the IDT, wavelength 10μm and a metallization ratio of 0.6 are shown in Figure 28. The thickness of the AlN film in this case was 4.3 microns.
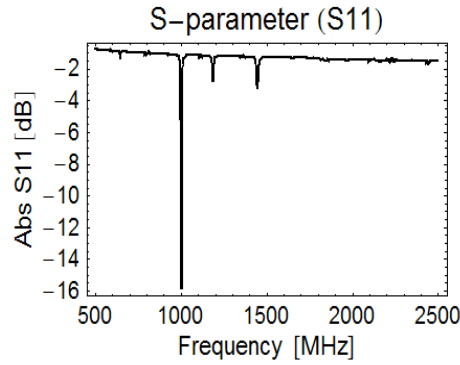
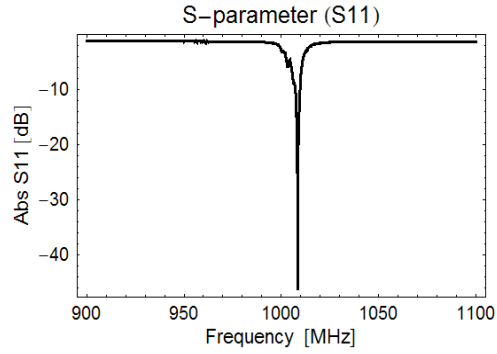**Figure 28** *Reflection coefficient of an AlN/Diamond resonator. The thickness of the AlN film was 4.3 μm.*

Four resonant peaks are clearly seen in the response. Comparing these results with the calculations in Figure 26 and Figure 27 above indicates that the first peak at 685MHz is a pure SAW mode (mode 0 in Figure 26 and Figure 27). Further, the resonance peaks at 1000, 1180 and 1445 MHz are identified as the second, third and fourth higher order SAW modes (modes 1, 2 and 3 respectively in the figures). Since the wavelength is 10μm the x-axis in Figure 28 and Figure 29 is readily translated to wave velocity in m/s by multiplying the frequency by a factor of 10. It is also noted that the velocity of the wave corresponding to the fourth peak at 1445 MHz exceeds that of the cut off velocity at 12.788 m/s in diamond which indicates that most likely this is a leaky SAW mode.

For test structure with an aperture of 400 microns, 801 electrodes in the IDT and a metallization ratio of 0.6, S_{11} outstanding values of −50dB were measured as shown in Figure 29.

Comparing the results shown in Figure 14 for the AlN/SiO$_2$/Si system with the ones shown here, the effect of a critical issue for thin film based electroacoustic devices, namely the electromagnetic feedthrough[61, 62] becomes apparent. Even using a SiO$_2$ intermediate layer, the parasitic capacitances between the IDT electrodes and the semiconducting Si substrate introduce high insertion loss levels in the frequency response. The response in contrast was dramatically improved when using diamond as a substrate.

Figure 29 *Reflection coefficient of an AlN/Diamond resonator. The thickness of the AlN film was 4.3 μm.*

To summarize the results for AlN/diamond it is most advantageous to utilize the 1st SAW mode which yields a coefficient of over 1%, and an extremely high SAW velocity between 10000 and 12000 m/s, which makes it suitable for the fabrication of SAW devices in the low to mid GHz frequency range using standard optical lithography.

Paper IX

This work focuses on the electroacoustic characterisation of AlN/diamond FSRAR resonators and in particular on the extraction of the Coupling of Modes (COM) parameters. COM is a phenomenological model of SAW propagation in grating structures which allows the determination of all important COM parameters such as SAW velocity, reflectivity from fingers, piezoelectric coupling, attenuation, etc. In general, these parameters can be derived from theoretical calculations (mainly based on the periodic Green function formalism) or extracted empirically. The advantage of the first approach is that the calculations are based solely on knowledge of the material constants (elasticity and piezoelectricity modules, dielectric constants, density, temperature derivatives, etc.) which are well known for most materials of interest, that is quartz, Lithium Niobate, and Lithium Tantalate, etc. In these cases the COM parameters to be derived directly from computer modelling and subsequently used for the design of SAW devices[63]. The biggest drawback is that it is a time consuming method, requiring a substantial processor power. Both computer modelling[40, 63] and data fitting[64-67] have been employed and reported in the literature.

It is noted that the second approach is, perhaps, more suitable for cases where the material constants are not exactly known, which is the case of thin polycrystalline films studied here. Thin films offer the unique possibility of combining the electroacoustic properties of the substrate with those of the film providing thus great flexibility. For instance, in this study we attempt to combine the excellent acoustic properties of polydiamond with the piezoelectric properties of AlN to achieve SAW devices, which are otherwise unachievable in either of the materials. This, as discussed above, necessitates the use of the empirical approach for the determination of the COM parameters.

Highly textured AlN films with several thicknesses have been grown on polycrystalline diamond and subsequently a variety of SAW resonator structures have been fabricated and characterised. Figure 30a shows the real part of the admittance of the SAW resonance peak for which we extract the COM parameters. This peak corresponds to the first SAW mode (see Figure 26 and Figure 27 above) for the case of 4.3μ-meter thick AlN film. The test structure in that case had an aperture of 200 microns, 801 electrodes in the IDT and a metallization ratio of 0.6, while the wavelength was 10 μm. The experimental curve (solid line) is fitted according to the COM model until a best fit is obtained (dashed line). As seen the simulated curve reproduces very well all significant details in the experimental one. It is noted that the COM model is a one-dimensional model and as such does not take into account two and three-dimensional effects. Thus, the slight increase in conductance between the main peak and the stop band is assumed to be due to contributions from secondary bulk waves generated through scattering at the edges of the electrodes. The peak on the left of the main response could not be identified positively and is thought to be a spurious response.
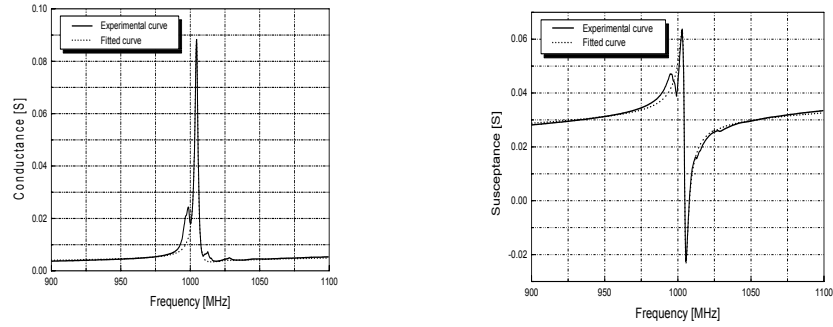
Figure 30 *Resonance peak of the test structure used for COM parameter extraction*
a) Real part. b) Imaginary part.

It is readily seen from Figure 30 that the SAW velocity is around 10000 m/s. For structures fabricated on 2μ-meter thick AlN this velocity is around 11800 m/s, which is more than 3 times higher than that on quartz. Thus for one and the same lithographic resolution such SAW devices will operate at three times higher frequencies. In addition, the effective coupling coefficient for the above resonators is of the order of 1%, which is again almost 10 times higher than that of quartz. Finally, a fairly high value of 500 has been obtained from the above procedure. Although this figure is significantly lower than that of quartz it is quite sufficient for a number of applications, most notably filters.

Table 2 summarises the most important COM parameters extracted from the fitting procedure:

COM - parameter	Value
SAW Velocity (V_0 [m/s])	10.143
Normalized transduction coefficient ($\alpha_n [\Omega^{-1/2}]$)	$1.0973 \cdot 10^{-4}$
Normalized Reflection coefficient (k_p)	$3.03 \cdot 10^{-2}$
Intrinsic attenuation γ_i [dB / λ]	$4.65 \ 10^{-2}$
Velocity dispersion (D)	20
Effective dielectric permittivity $\varepsilon_s(\infty)$ [F/m]	6.2×10^{-11}

Table 2 Values of the COM parameters extracted from the fitting procedure.

It is seen that the normalized transduction coefficient is 1.1×10^{-4}, which is a factor of three higher than that of quartz (3.3×10^{-5}). Further, the normalized transduction coefficient is readily converted to the so called unperturbed electromechanical coupling coefficient K_u^2 according to the Smith's definition[21] and is found to be $K_u^2 = 0.3\%$. Next, the intrinsic attenuation translates into an intrinsic material Q of 587. Note that this material Q corresponds to the composite AlN/diamond structure. The effective dielectric permittivity $\varepsilon_s(\infty)$ is around 6.2×10^{-11} F/m which, as expected, lies between that of diamond (5.5×10^{-11} F/m) and that of AlN (10×10^{-11} F/m).

Finally, the effective coupling coefficient, given by

$$(40) \qquad K_{eff}^2 = 2 \frac{f_a - f_r}{f_r}$$

where f_r and f_a are the resonance and antiresonance frequencies respectively, and the device Q, are extracted directly from the S_{11} measurements. The latter indicate a device Q of 579, which naturally is lower than the intrinsic Q, since it also includes additional parasitic losses, such as resistive, capacitive and inductive parasitics. The effective piezoelectric coupling coefficient K_{eff}^2 is 0.91%. Statistically, the device Q varied in the range 500 to 600, while K_{eff}^2 varied between 0.9% and 1.14% depending on the quality of the lithography process.

Acknowledgements

I would like to express my sincere gratitude to Prof. Sören Berg for giving me the opportunity to carry out my PhD studies. It meant a lot to me and I have no words to describe how thankful I am to him for that.

I can't find the right words either to express how thankful I am to Dr. Ilia Katardjiev, my supervisor during the five years of my thesis work. Thanks for both the financial and the great intellectual support as well as for believing in me even at times when I myself didn't do.

This work has been financially supported by the European Commission through an EU project IST-1999-11411.

I also would like to thank my sister Raquel; your seriousness while doing your PhD in Germany has helped me during these years.

I would like to thank my aunt Mila, for giving me the opportunity to study in Germany.

My dear Grandmother Julia, for all you taught me.

Thanks to Charlotte N. since without you I probably would have never gotten to know this beautiful country.

Sofia L. for being such a wonderful person as you are.

Jane C. for being so open and joyful; I owe you a visit to S.F.

Fredrik, my closest co-author and my tutor in Swedish for the work done.

Henrik et al. for all the great "wet etching" experiments at the Nations of Uppsala.

I also would like to thank Peter Schneider, a guy that helped me with my studies in Germany without asking for anything in return; I really appreciate that.

Raquel M., Juan Ramon and the rest my spanish friends at Uppsala, for all the good times we have had together.

All my friends from Pamplona; in spite of the distance, you have been closer to me than you can imagine.

German, for being so nice to talk to and for all the great times we had in our crazy-trips. Berlin, Glastonbury, Benicasim… not as wild as sitting at my desk at Ångström writing my thesis…but close to…

All my family, thanks for being there for me when I needed them.

Finally, I want to thank my dear mother; your hard work while raising the three of us all by yourself has inspired me and given me strength throughout my whole life.

Gonza.   Uppsala, March 2003.

References

[1] B. Drafts, "Acoustic wave technology sensors," *IEEE Transactions on Microwave Theory and Techniques*, vol. 49, pp. 795-802, 2001.

[2] B. L. Olutade and W. D. Hunt, "Sensitivity analysis of a thin film bulk acoustic resonator ladder filter," presented at Proceedings of International Frequency Control Symposium, New York, NY, USA Orlando, FL, USA, 1997.

[3] F. S. Hickernell, "Measurement techniques for evaluating piezoelectric thin films," presented at 1996 IEEE Ultrasonics Symposium. Proceedings, New York, NY, USA San Antonio, TX, USA, 1996.

[4] J. F. Rosenbaum, "Bulk Acoustic Wave Theory and Devices.," *Artech House*, 1988.

[5] A. Technologies, "Palo Alto, California," www.agilent.com.

[6] H. Goldstein, "Classical mechanics," Addison-Wesley, Ed., 1980, pp. 143-148.

[7] B. A. Auld, "Acoustic Fields and Waves in Solids, Volume I and Volume II.," *John Wiley & Sons*, 1973.

[8] J. J. C. a. W.R.Jones, "A method for estimating optimal crystal cuts and propagation directions for excitation of piezoelectric surface waves," *IEEE Trans. Sonics Ultrason.*, vol. SU-15, pp. 209-217, 1968.

[9] E. L. Adler, "Matrix methods applied to acoustic waves in multilayers," *IEEE Transactions on Ultrasonics, Ferroelectrics and Frequency Control*, vol. 37, pp. 485-90, 1990.

[10] Adler-EL, "SAW and pseudo-SAW properties using matrix methods," *IEEE-Transactions-on-Ultrasonics,-Ferroelectrics-and-Frequency-Control.*, vol. vol.41, no.6, Nov. 1994, pp. p.876-82, 1994.

[11] A. H. Fahmy and E. L. Adler, "Propagation of acoustic surface waves in multilayers: A matrix description," *Applied Physics Letters*, vol. 22, pp. 495-7, 1973.

[12] F. S. Hickernell and E. L. Adler, "Pseudo-SAW propagation on layered piezo-substrates: experiments and theory including film viscosity,"

presented at 1996 IEEE Ultrasonics Symposium. Proceedings, New York, NY, USA San Antonio, TX, USA, 1996.

[13]   A. H. Fahmy and E. L. Adler, "Multilayer acoustic-surface-wave program," *Proceedings of the Institution of Electrical Engineers*, vol. 122, pp. 470-2, 1975.

[14]   E. L. Adler, G. W. Farnell, J. Slaboszewicz, and C. K. Jen, "Interactive PC software for SAW propagation in anisotropic multilayers," presented at IEEE 1988 Ultrasonics Symposium. Proceedings (IEEE Cat. No.88CH2578-3), New York, NJ, USA Chicago, IL, USA, 1988.

[15]   E. L. Adler, J. K. Slaboszewicz, G. W. Farnell, and C. K. Jen, "PC software for SAW propagation in anisotropic multilayers," *IEEE Transactions on Ultrasonics, Ferroelectrics and Frequency Control*, vol. 37, pp. 215-23, 1990.

[16]   C. C. W. Ruppel, W. Ruile, G. Scholl, K. C. Wagner, and O. Manner, "Review of models for low-loss filter design and applications," presented at Proceedings of IEEE Ultrasonics Symposium, New York, NY, USA Cannes, France, 1994.

[17]   P. M. Smith, "Analysis techniques for surface acoustic wave devices," presented at 1997 SBMO/IEEE MTT-S International Microwave and Optoelectronics Conference. `Linking to the Next Century'. Proceedings, New York, NY, USA Natal, Brazil, 1997.

[18]   R. H. Tancrell and M. G. Holland, "Acoustic surface wave filters," *Proceedings of the IEEE*, vol. 59, pp. 393-409, 1971.

[19]   C. S. Hartmann, D. T. Bell, Jr., and R. C. Rosenfeld, "Impulse model design of acoustic surface-wave filters," *IEEE Transactions on Microwave Theory and Techniques*, vol. MTT-21, pp. 162-75, 1973.

[20]   D. C. Malocha, "Surface acoustic wave design fundamentals," presented at Proceedings of 6th International Microwave Conference (MIKON 96), Warsaw, Poland, 1996.

[21]   W. R. Smith, H. M. Gerard, J. H. Collins, T. M. Reeder, and H. J. Shaw, "Analysis of interdigital surface wave transducers by use of an equivalent circuit model," *IEEE Transactions on Microwave Theory and Techniques*, vol. MTT-17, pp. 856-64, 1969.

[22]   H. M. G. a. W. R. J. W.R.Smith, "Analysis and Design of Dispersive Interdigital Surface-Wave Transducers," *IEEE Transactions on microwave theory and techniques.*, vol. MTT-20, NO. 7, pp. 458-471, 1972.

[23]   W. F. P. W.R.Smith, "Fundamental and harmonic frequency circuit-model analysis of interdigital transducers with arbitrary metallisation ratios and polarity sequences," *IEEE Trans.*, vol. MTT-23, pp. 853-864, 1975.

[24]   Hickernell-TS, "Development of a SAW ladder filter for a portable phone system," *16th Piezoelectric Devices Conference and Exhibition. Electron. Ind. Assoc, Washington, DC, USA;*, vol. 2 vol. (vi+115+20) p.106-11 vol.1, 1994.

[25]   Y. Koyamada and S. Yoshikawa, "Coupled mode analysis for a long IDT," *Review of the Electrical Communication Laboratories*, vol. 27, pp. 432-44, 1979.

[26]   J. Koskela, V. P. Plessky, and M. M. Salomaa, "SAW/LSAW COM parameter extraction from computer experiments with harmonic admittance of a periodic array of electrodes," *IEEE Transactions on Ultrasonics, Ferroelectrics and Frequency Control*, vol. 46, pp. 806-16, 1999.

[27]   V. P. Plessky, S. N. Kondratiev, and C. Lambert, "Reduced passband ladder type SAW impedance element filters on strong piezoelectric substrates," presented at 1996 IEEE Ultrasonics Symposium. Proceedings, New York, NY, USA San Antonio, TX, USA, 1996.

[28]   E. L. Adler, M. P. da Cunha, and O. Schwelb, "Arbitrarily oriented SAW gratings: network model and the coupling-of-modes description," *IEEE Transactions on Ultrasonics, Ferroelectrics and Frequency Control*, vol. 38, pp. 220-30, 1991.

[29]   J. C. Andle, L. A. French, Jr., and J. F. Vetelino, "Theoretical and experimental results on two-port resonators fabricated on 36 degrees lithium tantalate," presented at Proceedings of the 1998 IEEE International Frequency Control Symposium (Cat. No.98CH36165), New York, NY, USA Pasadena, CA, USA, 1998.

[30]   J. Heighway, S. N. Kondratyev, and V. P. Plessky, "Impedance element SAW filters," presented at Proceedings of IEEE 48th Annual Symposium on Frequency Control, New York, NY, USA Boston, MA, USA, 1994.

[31]   P.-V. C.-D. Hartmann-CS, "'Patch' improvements to COM model for leaky waves," *IEEE Ultrasonics Symposium.Proceedings (Cat. No.94CH3468-6). IEEE, New York, NY, USA; 1994;*, vol. 3 vol. 1911 pp. p.297-300 vol.1., 1994.

[32]   P. Ventura and J.-M. Hode, "A new accurate analysis of periodic IDTs built on unconventional orientation on quartz," presented at 1997 IEEE

Ultrasonics Symposium Proceedings An International Symposium, New York, NY, USA, 1997.

[33]   J. Koskela, J. Fagerholm, D. P. Morgan, and M. M. Salomaa, "Self-consistent analysis of arbitrary 1D SAW transducers," presented at 1996 IEEE Ultrasonics Symposium. Proceedings, New York, NY, USA San Antonio, TX, USA, 1996.

[34]   Peach-RC, "A general Green function analysis for SAW devices," *IEEE Ultrasonics Symposium.Proceedings. An International Symposium (Cat. No.95CH35844). IEEE, New York, NY, USA; 1995*, vol. 2 vol. 1636 pp. p.221-5 vol.1. Publication Year, 1995.

[35]   R.C.Peach, "A general approach to the electrostatic problem of the SAW interdigital transducer," *IEEE Trans*, vol. SU-28, pp. 96-105, 1981.

[36]   P. M. Smith, "Dyadic Green's functions for multi-layer SAW substrates," *IEEE Transactions on Ultrasonics, Ferroelectrics and Frequency Control*, vol. 48, pp. 171-9, 2001.

[37]   B.-S. Weihnacht-M, "The effective permittivity in the complex plane and a simple estimation method for leaky wave slowness," *IEEE Ultrasonics Symposium Proceedings (Cat.No.96CH35993). IEEE, New York, NY, USA; 1996;*, vol. 2 vol. 1622 pp. p.221-4 vol.1., 1996.

[38]   P.-V. Thorvaldsson-T, "Periodic Green's functions analysis of SAW and leaky SAW propagation in a periodic system of electrodes on a piezoelectric crystal," *IEEE-Transactions-on-Ultrasonics,-Ferroelectrics-and-Frequency-Control.*, vol. vol.42, no.2; March 1995, pp. p.280-93, 1995.

[39]   P. Ventura, J. Desbois, and L. Boyer, "A mixed FEM/analytical model of the electrode mechanical perturbation for SAW and PSAW propagation," presented at Proceedings of IEEE Ultrasonics Symposium, New York, NY, USA, 1993.

[40]   V.-P. H.-J. Solal-M, "A new efficient combined FEM and periodic Green's function formalism for the analysis of periodic SAW structures," *IEEE Ultrasonics Symposium.Proceedings. An International Symposium (Cat. No.95CH35844). IEEE, New York, NY, USA; 1995*, vol. 2 vol. 1636 pp. p.263-8 vol.1, 1995.

[41]   P. Ventura, J. M. Hode, M. Solal, J. Desbois, and J. Ribbe, "Numerical methods for SAW propagation characterization," presented at 1998 IEEE Ultrasonics Symposium. Proceedings, Piscataway, NJ, USA Sendai, Japan, 1998.

[42]   P. Ventura, J. M. Hode, J. Desbois, and H. Solal, "Combined FEM and Green's function analysis of periodic SAW structure, application to the calculation of reflection and scattering parameters," *IEEE Transactions on Ultrasonics, Ferroelectrics and Frequency Control*, vol. 48, pp. 1259-74, 2001.

[43]   Y. Zhang, J. Desbois, and L. Boyer, "Characteristic parameters of surface acoustic waves in a periodic metal grating on a piezoelectric substrate," *IEEE Transactions on Ultrasonics, Ferroelectrics and Frequency Control*, vol. 40, pp. 183-92, 1993.

[44]   H.-K. Yamaguchi-H, "General-purpose simulator for leaky surface acoustic wave devices based on coupling-of-modes theory," *IEEE Ultrasonics Symposium Proceedings (Cat.No.96CH35993). IEEE, New York, NY, USA; 1996;*, vol. 2 vol. 1622 pp. p.117-22 vol.1., 1996.

[45]   K.-Y. Hashimoto and M. Yamaguchi, "Derivation of coupling-of-modes parameters for SAW device analysis by means of boundary element method," presented at IEEE 1991 Ultrasonics Symposium Proceedings. (Cat. No.91CH3079-1), New York, NY, USA Orlando, FL, USA, 1991.

[46]   B. P. Abbott, "A derivation of the coupling-of-modes parameters based on the scattering analysis of SAW transducers and gratings," presented at IEEE 1991 Ultrasonics Symposium Proceedings. (Cat. No.91CH3079-1), New York, NY, USA Orlando, FL, USA, 1991.

[47]   J. D. Larson, III., P. D. Bradley, S. Wartenberg, and R. C. Ruby, "Modified Butterworth-Van Dyke circuit for FBAR resonators and automated measurement system," presented at 2000 IEEE Ultrasonics Symposium. Proceedings. An International Symposium, Piscataway, NJ, USA San Juan, Puerto Rico, 2000.

[48]   M. Ylilammi, J. Ella, M. Partanen, and J. Kaitila, "Thin film bulk acoustic wave filter," *IEEE Transactions on Ultrasonics, Ferroelectrics and Frequency Control*, vol. 49, pp. 535-9, 2002.

[49]   "IEEE standard on piezoelectricity," 1988.

[50]   E. B. H.Nowotny, "General one-dimensional treatment of the layered piezoelectric resonator with two electrodes," *J.Acoust.Soc Am.*, vol. 82, pp. 513-521, 1987.

[51]   E. B. H.Nowotny, "Layered piezoelectric resonators with an arbitrary number of electrodes (general one-dimensional treatment)," *J.Acoust.Soc Am.*, vol. 90, pp. 1238-1245, 1991.

[52]   D. W. Pashley, M.J.Stowell, M.H.Jacobs, and T.J.Law, vol. 10: 127, 1964.

[53]   S. Berg, T. Nyberg, H.-O. Blom, and C. Nender, "Computer modeling as a tool to predict deposition rate and film composition in the reactive sputtering process," *Journal of Vacuum Science & Technology A (Vacuum, Surfaces, and Films)*, vol. 16, pp. 1277-85, 1998.

[54]   K. Macak, T. Nyberg, P. Macak, M. K. Olsson, U. Helmersson, and S. Berg, "Modeling of the deposition of stoichiometric Al/sub 2/O/sub 3/ using nonarcing direct current magnetron sputtering," *Journal of Vacuum Science & Technology A (Vacuum, Surfaces, and Films)*, vol. 16, pp. 1286-92, 1998.

[55]   G. F. Iriarte, F. Engelmark, and I. V. Katardjiev, "Reactive sputter deposition of highly oriented AlN films at room temperature," *Journal of Materials Research*, vol. 17, pp. 1469-75, 2002.

[56]   L. B. Jonsson, C. Hedlund, I. V. Katardjiev, and S. Berg, "Compositional variations of sputter deposited Ti/W barrier layers on substrates with pronounced surface topography," *Thin Solid Films*, vol. 348, pp. 227-32, 1999.

[57]   D. B. Bergstrom, F. Tian, I. Petrov, J. Moser, and J. E. Greene, "Origin of compositional variations in sputter-deposited Ti/sub x/W/sub 1-x/ diffusion barrier layers," *Applied Physics Letters*, vol. 67, pp. 3102-4, 1995.

[58]   P. Martensson and A. Harsta, "Halide chemical vapour deposition of Bi/sub 2/Sr/sub 2/CaCu/sub 2/O/sub 8+x/: aspects of epitaxy," *Journal of Crystal Growth*, vol. 156, pp. 67-73, 1995.

[59]   K. Sato, S. Umino, K. Tsubouchi, and N. Mikoshiba, "Low temperature growth of epitaxial AlN films on sapphire," presented at IEEE 1985 Ultrasonics Symposium. Proceedings. (Cat. No.85CH2209-5), New York, NY, USA, 1985.

[60]   K. Tsubouchi and N. Mikoshiba, "Zero-temperature-coefficient SAW devices on AlN epitaxial films," *IEEE Transactions on Sonics and Ultrasonics*, vol. SU-32, pp. 634-44, 1985.

[61]   F. Moller and W. Buff, "Electromagnetic feedthrough in Si/ZnO-SAW-devices," presented at IEEE 1992 Ultrasonics Symposium (Cat. No.92CH3118-7), New York, NY, USA Tucson, AZ, USA, 1992.

[62]   J. H. Visser and A. Venema, "Silicon SAW devices and electromagnetic feedthrough," presented at IEEE 1988 Ultrasonics Symposium. Proceedings (IEEE Cat. No.88CH2578-3), New York, NJ, USA Chicago, IL, USA, 1988.

[63]   P. Ventura, P. Dufilie, and S. Boret, "The effect of the fabrication process in propagation and reflectivity in an IDT," presented at 1996 IEEE Ultrasonics Symposium. Proceedings, New York, NY, USA San Antonio, TX, USA, 1996.

[64]   C. S. Hartmann and V. P. Plessky, "Experimental measurements of propagation, attenuation, reflection and scattering of leaky waves in Al electrode gratings on 41 degrees , 52 degrees and 64 degrees -LiNbO/sub 3/," presented at Proceedings of IEEE Ultrasonics Symposium, New York, NY, USA Baltimore, MD, USA, 1993.

[65]   V. P. Plessky and C. S. Hartmann, "Characteristics of leaky SAWs on 36-LiTaO/sub 3/ in periodic structures of heavy electrodes," presented at Proceedings of IEEE Ultrasonics Symposium, New York, NY, USA Baltimore, MD, USA, 1993.

[66]   J. H. Hines and D. C. Malocha, "A simple transducer equivalent circuit parameter extraction technique," presented at Proceedings of IEEE Ultrasonics Symposium, New York, NY, USA Baltimore, MD, USA, 1993.

[67]   M.-A. S. V. P. Plessky, S. N. Krasnikova, "Exact material parameter extraction for narrow band filters and resonators designed on quartz," presented at Proc. of the 8th EFTF - 94, Munich, 1994.